

c. 2
**OPTIMUM BIRD FLOCK SIZE IN
FORMATION FLIGHT**

By

MRIGESH KSHATRIYA

B.Sc., The University of British Columbia

**A THESIS SUBMITTED IN PARTIAL FULFILLMENT OF
THE REQUIREMENTS FOR THE DEGREE OF
MASTER OF SCIENCE**

in

**THE FACULTY OF GRADUATE STUDIES
(Department of Zoology)**

We accept this thesis as conforming
to the required standard

THE UNIVERSITY OF BRITISH COLUMBIA

June 1990

© Mrigesh Kshatriya, 1990

In presenting this thesis in partial fulfilment of the requirements for an advanced degree at the University of British Columbia, I agree that the Library shall make it freely available for reference and study. I further agree that permission for extensive copying of this thesis for scholarly purposes may be granted by the head of my department or by his or her representatives. It is understood that copying or publication of this thesis for financial gain shall not be allowed without my written permission.

Department of Zoology

The University of British Columbia
Vancouver, Canada

Date July, 11 1990

Abstract

A theoretical model of flock size in migrating birds is developed. Although previous models of formation flight in birds show improved flight performance, they do not explain flock size variation across bird species or at different times of the year for a given bird species. This model captures some of the diversity in flock size observed in nature by incorporating energetic costs of flight and energy income from foraging. It turns out that within a myriad of possible flock sizes there is one that is optimal for maximizing energetic efficiency (net energetic gain/energy expenditure) for a given maximum range speed, which minimizes flying cost per unit distance flown, and under certain migration conditions (i.e. flight distance and total time to complete the journey). Net energetic gain from foraging equals the rate of prey encountered times the time spent foraging. Energy expenditure from flying is determined from formation flight theory for a fixed wing aircraft. The benefit of formation flight, as derived from an approximation technique, is represented in close-form. This expression is a function of flock size and wing-tip spacing (WTS) and simplifies flight cost calculations. Under certain WTS, a good approximation to the induced drag for a member of a flock of size n is $1/n$ th of the induced drag of a single bird. In addition, optimum flight speed of a flock is $(1/n)^{1/4}$ of the optimum flight speed of a single individual.

The approach taken here allows the prediction of flock size in migrating birds. Model results are discussed in relation to observation of flock size under various migration conditions. If migration is constrained by hours of daylight, seasonal variation in flock size is expected if the start time of the north and southward migration are asymmetrical with respect to the summer solstice (June 21). Under certain conditions, such as long non-stop migration, solo flight is an optimum migratory strategy.

Table Of Contents

Abstract	ii
List of Figures	v
List of Tables	ix
List of Symbols	x
Acknowledgements	xii
Introduction	1
Aerodynamics of Bird Flight	4
<i>Solo Flight</i>	4
<i>Quasi-steady Assumption</i>	4
<i>Analysis of Steady Horizontal Flight</i>	5
<i>Formation Flight</i>	7
<i>Flow Field in the Neighborhood of an Airfoil</i>	7
<i>Upwash Velocity Calculations</i>	18
<i>Induced Drag Reduction</i>	18
<i>Approximation Formula</i>	27
Model	45
<i>Energy Expenditure</i>	45
<i>Energy Gain</i>	46
<i>Ratio of Energy Gain to Energy Expenditure</i>	47
Results	49
<i>Conditions for Solo Flight</i>	49

<i>Optimum Flock Size and Wing-tip Spacing</i>	52
<i>Optimum vs Maximum Flock Size</i>	52
<i>Effect of U_{mr} on Optimum Flock Size</i>	55
<i>Seasonal Variation and Optimum Flock Size</i>	58
Discussion	69
<i>Aerodynamic Model</i>	69
<i>Optimum Flock Size Model</i>	73
Summary	80
References	81
Appendices	88
A. <i>Limiting Case as $n \rightarrow \infty$</i>	88
B. <i>Approximation Technique</i>	89
C. <i>Optimum Flock Size vs Wing-tip Spacing</i>	91
D. <i>Upper Bound for Maximum Flock Size</i>	93

List of Figures

- Figure 1.** Evolution of tip vortices behind a wing of finite span (based on Tokaty, 1971). See text for detail. 9
- Figure 2.** A unique circulatory flow ($v = \Gamma/2\pi r$) superimposed (added) to the free stream flow (U) mimics the flow around a lifting wing. 12
- Figure 3.** Circulation (Γ) superimposed on forward velocity (U) and downwash (w_d) to produce lift (L) and induced drag (D_I) respectively (Houghton & Brock, 1960). 15
- Figure 4.** Wing with rolled-up vortex sheet (left) and its equivalent horseshoe vortex: bound vortex ($|||$) and tip vortex (\equiv). 17
- Figure 5.** Vertical flow in the vicinity of a lifting wing, moving in the positive x direction. The wing tips are at points $x = 0$ and $y = \pm 1$ 20
- Figure 6.** Distribution of $n = 5$ birds and their horseshoe vortex on the x - y plane. Starting from the left, each bird is numbered from 1 to n . The distance, as projected on the y -axis, between bird number i and j is $\delta y_{ij} = |i - j|(2b + s)$, where b is the semi-wing span and s is the distance between adjacent birds perpendicular to the flight path. Each bird is of span $2b$, represented by a bound vortex of length $2a$, where $a = \pi/4b$ 26
- Figure 7.** Ratio of induced drag in formation to solo flight, as a function of flock size, n , and various wing-tip spacing, s , as a percent of the semi-wing span (solid). Curves are shown for $s/b = +100, +50, +10, 0, -10, -15$, and -20% . For the special case when the wing-tip spacing is such that the tip vortices of the two adjacent birds overlap ($s = 2(a - b)$) the ratio is given by the dash line. 29
- Figure 8.** Percent contribution to the total induced drag reduction of the left most bird (Bird 1) by the neighboring birds numbered 2 through 15 (bottom x -axis), flying in abreast formation with a wing-tip spacing equal to zero ($s = 0$). The top

axis is the distance of each bird as measured from Bird 1. Each bird is assumed to be of unit semi-span ($b = 1$). 32


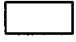


Figure 9. Pictorial representation of the approximation technique for $n = 6$ birds, solid plus one diagonal filled wing. (A & C) The left and right most birds in the vee formation () are assumed to be flanked on the opposite leg by an infinite number of birds (...). (B) Each bird inside a flock, for example , is assumed to be flanked by an infinite number of birds on both legs of the vee (...). 35

Figure 10. Effect of flock size and spacing ratio, s/b , on relative error as result of the approximation technique. Curves are shown for $s/b = -20, -15, -10, 0, +10, +50$, and $+100\%$ 38

Figure 11. Induced drag in formation flight, $\bar{D}_I(n)$, relative to that in solo flight, D_I , for $n = 2, 3, 9, 25$ and infinite number of birds. 40

Figure 12. Air flow pattern, as represented by a horseshoe vortex, of two wings each of semi-span b , located at wing-tip spacing $s = 2(a - b)$. Due to the positioning, tip vortex of the lead bird cancels the tip vortex of the second bird (A). The resulting flow, as shown by the horseshoe vortex in (B), is equivalent to a flow created by a single wing of span $2b$ 43

Figure 13. Condition for solo flight depends on the value of d , U_{mr} and T . For a given U_{mr} , a solid line divides the values of d and T pairs that predict solo flight (below the line) from d and T pairs that predict optimum flock size greater than one (above the line). To illustrate, say $U_{mr} = 1/2$, (T, d) pairs that fall in the grey region correspond to solo flight while pairs that fall in the white region correspond to formation flight. 51

Figure 14. Optimum flock size is plotted against T/t_a . Curves correspond to wing-tip spacing, expressed by a non-dimensional ratio, s/b ($+100, +50, +20, 0$,

-10, -20%). Smallest flock size occurs at wing-tip spacing $s = 2(a - b)$ (dash line), flock configuration for maximum induced drag reduction. 54

Figure 15. Normalized relative to a solo flyer, equation 59 is plotted against different flock sizes, n . The benefit of flying in a flock of size $n = n_*$ is identical to that of flying solo: $R(1) = R(n_*)$. In this example, a member of a flock of size $n = n_{opt}$ is 60% more efficient than a solo flyer. 57

Figure 16. Effect of T , d and U_{mr} on optimum flock size. Each panel, from left to right, is for a fixed T , 6, 12, and 18 hrs respectively, and is a plot of flock size vs distance, d (km) for $U_{mr} = 18, 36$ and 54 km/hr (1 – 3 respectively). Solid horizontal line corresponds to $n_{opt} = 1$, solo flight. 62

Figure 17. Contour of day length (hrs) with time of year and with latitude (solid lines). The dashed zigzag lines represent movement, from 10°N to 50°N , of two hypothetical migratory bird species. By flying equidistant number of days before and after the summer solstice (top axis), species A (short dash) will experience the same hour of day length on both the north and southward migration; consequently, no seasonal variation in flock size is to be expected. If the two phases occur in an asymmetrical pattern, as for species B (long dash), the average day length during the northward migration will be larger than the day length during the southward migration; as a result, seasonal variation in flock size is to be expected. The degree of variation in flock size is plotted in figure 18. 65

Figure 18. For migration from 10°N to 50°N , contours of the ratio R_s are plotted against t_b and t_r . The ratio R_s for bird species A and B is determined by the value of (t_b, t_r) pair which is (30,30) and (30,120) days respectively (see Figure 17). Ratio $R_s < 1$ corresponds to flock sizes being smaller during the southward migration compared to that during the northward migration. A ratio of one implies that flock sizes during the north and south migration are identical. 68

Figure 19. Percent reduction in optimum flight speed relative to a single bird ($[U_{mr} - U_{mr}(n)]/U_{mr}$) at different flock size, n , and spacing index, s/b (s is WTS,

b is semi-wing span). The solid line corresponds to a WTS when trailing vorticies of adjacent bird cancel each other out. 72

Figure 20. Predicted optimum flock size during the spring and autumn migration for varying distances between stop-over sites (top axis) or equivalentley the nubmer of stop-overs required to complete the 855 km journey (bottom axis). See text for detail. 78

List of Tables

Table 1. Relation of maximum range speed to body mass, after Greenwalt (1962, 1975) and Rayner (1979). Optimum flock size is shown divided by $[T/d]^4$. (All quantities in MKS units.) 60

List of Symbols

s wing tip spacing

b semi wingspan

A aspect ratio $\equiv (2b)^2/S$

$C_{D(pro)}$ parasite (body) drag coefficient

$C_{D(para)}$ profile (body) drag coefficient

S area of the wings

A_p frontally projected area of the body

m mass

g gravitational acceleration (9.8m/s²)

ρ air density

U forward velocity

U_{mr} speed for maximum range

D_P parasite (body) + profile (wing) drag

D_I induced drag

L lift force

k_p a constant associated with parasite and profile drag

k_i a constant associated with induced drag

n number of birds in a flock

D total drag force acting on a bird

$\bar{D}_I(n)$ flock average induced drag

$U_{mr}(n)$ maximum range speed for flock of size n

E_{fly} energetic cost of flying

E_{out} energetic cost of flying in formation flight

E_{in} net energy gain from foraging

R ratio of energy gain to energy expenditure

λ number of prey (energy units) per unit time

Γ circulation strength

w vertical velocity component

d flight distance

t_a airborne time

t_p time spent in a patch

T total time available $\equiv t_p + t_a$

n_{opt} optimum flock size number

n_* maximum flock size number

t_j julian date (0 = Jan. 1, 1 = Jan. 2, ...)

$\delta(t_j)$ solar declination as a function of julian date

H day length, hours between sunrise and sunset

ℓ latitude

ℓ_1, ℓ_2 beginning and ending latitudes of the migration

t_b, t_r beginning and returning time of the migration

R_s ratio of expected flock size variation with season

Acknowledgements

I would like thank Dr. R. W. Blake for his support. Special thanks to Rebbeca Kolotylo and horacio de la cueva for allowing access to their large collection of scientific papers. I would also like to thank the BDC staff for computing assistance.

Introduction

A great many birds migrate in flocks. The most characteristic migratory formation is a reversed V, apex in the direction of flight. "The birds are usually ordered in swept lines and they keep so small a span wise distance that the wing-tips of two adjoining birds lie about one behind the other" (Hummel, 1983). This mode of formation flight is typical of geese, ducks, pelicans, cranes, and shore-birds (Dorst, 1962). Formation flight, however, is not common to all migratory species. Some birds, such as the cuckoos, nitejars, orioles, numerous birds of prey, journey alone (Dorst, 1962). The reason why some species of birds adopt formation flight and others do not is not clear. Furthermore, the advantage of flying in this fashion is also unclear. Numerous explanations have been offered, however.

Fransiket (1951) purposed that formation flight allows for good optical contact and thus decreased risk of collision. It may, on the other hand, function to decrease risk of predation, a function similar to that suggested for schooling in fish (Vine, 1971; Weihs, 1973). Equally, formation flight may allow older birds with previous migratory experience to act as navigators for the inexperienced birds of the flock (Dorst, 1962). It has been suggested that formation flight may assist navigation by averaging the direction preference of individual birds (Heppner, 1974) although contradictory information was reported by Keeton (1970). Another possibility is that formation flight, as with airplanes, may provide aerodynamic benefit over solo flight. Early aviators noted that patrol leaders burned significantly more fuel than the other planes in the formation (Dorst, 1962; Houghton & Brock, 1960).

While many explanations have been put forward for formation flight in birds, the aerodynamic hypothesis allows for quantifiable energetic savings. Weiselsberger (1914) was the first to give the correct description of the power reduction for formation flight. Flight tests with formations of two airplanes show that the power reduction was in close agreement with that predicted by aerodynamic theory (Hummel & Beukenberg, 1989). The aerodynamic rationale for formation flight

is that while each wing creates lift by generating downward momentum within its span, an upwash is created beyond the wing. In a vee formation, each bird flies in an upwash field generated by all other wings in the formation. This is equivalent to flying in an upcurrent and consequently each member of the flock experiences a reduction in flight power. The magnitude of the power reduction depends on wing tip spacing, and on the number of birds in the flock.

In a quantitative analysis, Lissaman and Schollenberger (1970) plotted the reduction in power of formation flight of 3, 9, 25 and an infinite number of birds showing that as the flock size increases flight power requirement decreases. Consequently, their results imply that in order to minimize flying cost birds should fly in a formation of infinite size! Although this is a meaningless statement, the corollary which follows is that birds should fly in the largest flock possible. In particular, two or more flocks should not fly beside each other but rather join to form a single large flock. However, numerous flocks of Snow Geese (*Anser caerulescens*) were observed flying beside each other at the Riefel Island Bird Sanctuary. While individuals may sometimes change flock arrangement in mid air, flocks do not merge to form a single large flock. More importantly, Lissaman and Schollenberger (1970) results do not explain avian flock size variation observed across species. For example, some species of birds such as the common heron that nest in large colonies have the opportunity to form large flocks often migrate in groups of only a few birds (Dorst, 1962). On the other hand, some species of birds migrate in large flocks, even if they are normally solitary (McFarland, 1987). In addition, some migrants, such as wild ducks and geese travel in small numbers. Other species such as Short-eared owl (*Asio flammeus*) and Scops Owls (*Ofus scops*) often fly in large numbers. Black Storks migrate in flocks of sixty to seventy, whereas there are often fifty to 100 Brant geese (*Branta bernicla*) and 500 to 1,000 common scoters (*Oidemia nigra*) in a flock (Dorst, 1962).

The aim of this study is to show that there is an optimal flock size for birds during migration. This is done by quantifying the flight energetics of formation

flight and foraging energetics. Taking the energy expenditure of formation flight and energy gain of foraging together, the model shows that optimum flock number is a function of morphological parameters of the bird, flight distance, and total time available for migration. Since optimum flock size is a function of the three variables mentioned above, it is also possible to predict, among other things, under what conditions solo flight is more advantageous than formation flight.

Aerodynamics of Bird Flight

Solo Flight

Quasi-steady Assumptions

The aerodynamics of flapping bird flight can be based on the quasi-steady approach: that the instantaneous aerodynamic forces on a flapping wing are those that a wing would experience in steady motion at the same instantaneous speed and angle of attack (Ellington, 1984). In other words, it is assumed that averaged over the wing-beat cycle, the aerodynamic forces are of the same magnitude as that of a fixed wing. The aerodynamic forces may be subdivided into four components, profile, parasite and induced drag, plus the drag created by the unsteady motion of the wing. The profile and parasite drag is determined by the wetted surface area of the wing and by the degree of streamlining of the body, respectively. Collectively called the profile drag, it is proportional to the velocity square. Induced drag is associated with generation of lift forces and is inversely proportional to the square of the velocity. During optimal cruising flight speed, profile and induced drag are of equal magnitude (Pennycuik, 1972). However, the fourth term, related to flapping motion, is of low magnitude if the reduced frequency, ratio of tip flapping speed to the flight speed, is low (Lissaman & Shollenberger, 1970).

Spedding (1987) studied the structure of a wake behind a kestrel (*Falco tinnunculus*) in flapping flight using stereophotogrammetry of multiple flash photographs of the motion of small soap-covered helium bubbles. His findings showed that at moderate flight speeds the rate of momentum generated in the wake approximated that of the quasi-steady state model. Spedding, concludes that "on occasion where an estimate of the induced power requirement at moderate flight speeds is required as a component in the calculation of the energy budget of a flying bird, the added complexity of a more rigorous and complete aerodynamic model is not justified by the small improvement in accuracy in estimating one component of the total aerodynamic power requirement." In the case of a kestrel of mass $m = 0.12 \text{ kg}$ the reduced

frequency was calculated to be ≈ 1 . From allometric equations given by Pennycuick (1972) and Rayner (1979a) it can be shown that reduced frequency $\propto 1/m^{1/6}$. In other words reduced frequency decreases with mass of the bird. If the wing beat kinematics of the kestrel are taken to be representative of birds of similar or lower reduced frequency (i.e. greater mass) then the quasi-steady model can be applied to estimate bird flight energetics. However, in the flight of small passerines where reduced frequency is relatively high, unsteady aerodynamic effects due to flapping become important (Kokshaysky, 1979; Ellington, 1984).

As a first approximation to the energy budget of a flying bird the cyclic variation in flapping flight is assumed to be of second order and therefore is ignored. In short, the average aerodynamic drag experienced by a bird during flapping flight is assumed to be equivalent to drag on a bird with fixed wings in the horizontal position. The following analysis applies to fixed wing flight on the basis of classical aerodynamic theory (Pennycuick, 1969,1972,1978; Rayner 1979a).

Analysis of Steady Horizontal Flight

Aerodynamic drag in steady horizontal flight may be expressed in the form

$$D = D_P + D_I \quad (1)$$

where D_P is the sum of the parasite and profile drag and D_I is the induced drag. The parasite and profile drag are given by

$$D_P = \frac{1}{2}\rho S C_{D(pro)} U^2 + \frac{1}{2}\rho A_p C_{D(para)} U^2 \quad (2)$$

where ρ is the air density, U is the flight speed, S is the wing area and A_p is the frontal projected area of the body; $C_{D(pro)}$ is the drag coefficient of the body and $C_{D(para)}$ is the drag coefficient of the wings. The induced drag may be written as

$$D_I = \frac{L^2}{2\pi\rho b^2 U^2} \quad (3)$$

where L is the lift force generated by the wings; b is the semi-wing span. The total drag on a bird flying at a constant speed U is

$$D = \frac{1}{2}\rho S C_{D(pro)} U^2 + \frac{1}{2}\rho A_p C_{D(para)} U^2 + \frac{L^2}{2\pi\rho b^2 U^2} \quad (4)$$

For the case of horizontal flight the lift force balances the weight of the bird, in other words

$$L = mg \quad (5)$$

where m is the mass of the animal and g is the gravitational acceleration (9.8 m/s^2).

Grouping parameters, equation (4) can be written as

$$D = k_p U^2 + k_i U^{-2} \quad (6)$$

where

$$k_p = \frac{1}{2}\rho S C_{D(pro)} + \frac{1}{2}\rho A_p C_{D(para)} \quad \text{and} \quad k_i = \frac{(mg)^2}{2\pi\rho b^2} \quad (7)$$

The total aerodynamic force acting on a bird flying at constant speed U is given by equation (6). The energy required to fly a distance d is

$$E_{fly} = D \cdot d. \quad (8)$$

Flight energy in relation to forward speed follows a U-shaped curve. At higher velocities the parasite and profile drag become the dominant terms; while at lower velocities the induced drag dominantes. As a result there is a speed at which energy expenditure for flight is at a minimum.

Specifically, the cruising speed, which minimizes flying cost per unit distance travelled, is calculated by differentiating (E_{fly}/d) , and setting the first derivative equal to zero:

$$\frac{d}{dU} \frac{E_{fly}}{d} = 0 = 2k_p U - 2k_i U^{-3}. \quad (9)$$

Solving the above equation for U gives

$$U_{mr} = \left[\frac{k_i}{k_p} \right]^{1/4}. \quad (10)$$

Optimum Bird Flock Size in Formation Flight

In migratory flight, cruising speed, which minimizes energy consumption per unit distance flown, allows migrants to cover the maximum range on a given energy reserve. Speeds from radar studies, collected by Alerstam (1976), show that mean air speed (flight speed corrected for influence of wind) of migrants is generally close to the predicted cruising speed, U_{mr} . The maximum range speed should be used whenever the longest distance should be covered on a given amount of energy.

Formation Flight

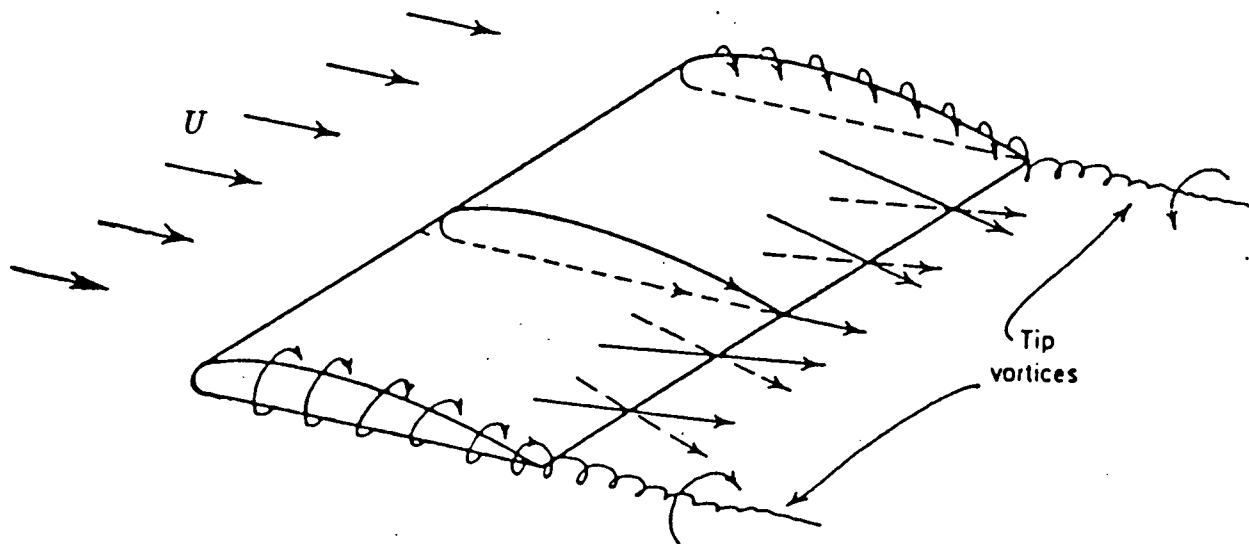
Flow Field in the Neighborhood of an Airfoil

In order to quantify the savings obtained in formation flight, it is necessary to model the flow close to a airfoil. The most common approach used is the horseshoe vortex model. A vortex is a "core" of rotating fluid, around which air flows in concentric circles (Houghton & Brock, 1960). In the model, the airfoil is replaced by a bound vortex, and the trailing wake is replaced by two tip vortices.

Under the right conditions, tip vortices can be seen behind an airfoil. The formation of these trailing vortices can be explained as follows. The pressure on the upper surface of a wing is smaller than that on the lower surface of a lifting wing. A pressure gradient exists between the upper and lower surfaces which equalizes beyond the wing tips. The tendency of the air is to equalize any pressure difference; as a result, air "leaks" to the top from the bottom of the wing, from the region of high pressure to the region of low pressure. This pressure equalization at the wing tips causes an inward deflection of the streamlines above the wing and an outward deflection below the wing (Figure 1).

The difference in spanwise velocity will cause air to roll up in into a number of small vortices (a vortex sheet), distributed along the wing span. A short distance downstream the vortices roll up and combine into two distinct cylindrical vortices. These two vortices, referred to as tip vortices, rotate in opposite directions and form

Figure 1. Evolution of tip vortices behind a wing of finite span
(based on Tokaty, 1971). See text for detail.



just inboard of the wing-tips. The distance between the two tip vortices is $2a$ where $a \approx \frac{\pi}{4}b$ and b is the semi-wing span (Higdon & Corrsin, 1978).

Whereas the tip vortices can be easily verified visually, the bound vortex is a useful theoretical abstraction to simulate accurately all the properties of a real airfoil. In general, lift produced by a wing is explained from the fact that airflow is accelerated over the top surface of a wing while that flowing below is decelerated relative to the free stream. The difference in speed, by Bernoulli's theorem, results in reduced pressure above the wing and increased pressure below it, and this pressure difference is what supports the weight of the wing. The difference in speed above and below the airfoil can be resolved into a circulatory flow, centered at the wing, superimposed on the free-stream. Circulatory flow is created by replacing the airfoil by a bound vortex, which causes air to flow in concentric circles outside its core. The pictorial equation of figure 2, shows that a free stream flow plus the flow due to the bound vortex creates a flow identical to one at an airfoil. The bound vortex can be considered as a rigid rotating body (rotating cylinder) (Prandtl & Tietjens, 1957). The strength of the vortex, Γ (m^2/s), is defined as

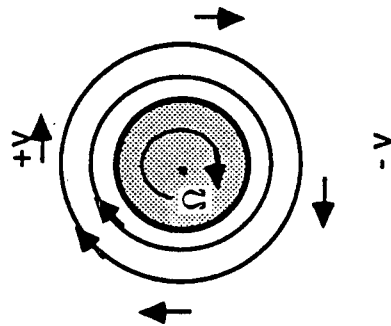
$$\Gamma = 2\pi\Omega r^2, \quad (11)$$

where Ω is the angular velocity and r is the radius of the core (Prandtl & Tietjens, 1957). Replacing the airfoil by a vortex, which acts like a rotating cylindrical body, not only describes the flow at an airfoil but also allows the calculation of the lift force and the induced drag created by the airfoil.

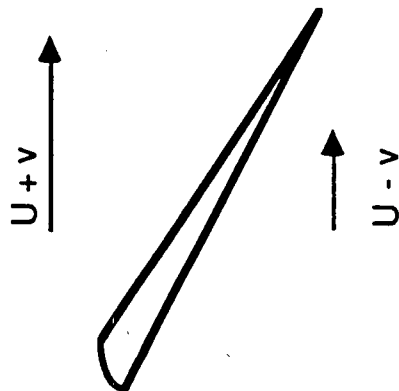
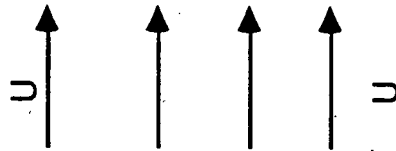
A "sideways" force associated with a spinning object moving through the air has been recognized since ancient times (Houghton & Brock, 1960). It is usually referred to as the Magnus effect. In the case of the horseshoe vortex model, the spinning cylinder, or the bound vortex, will create a lift force perpendicular to the free-stream velocity. The lift force created per unit span, L' , is

$$L' = \rho\Gamma U. \quad (12)$$

Figure 2. A unique circulatory flow ($v = \Gamma/2\pi r$) superimposed (added) to the free stream flow (U) mimics the flow around a lifting wing.



+



This expression is the algebraic form of the Kutta-Zhukovsky Theorem, and is valid for any system where circulation is superimposed on a uniform velocity (Houghton & Brock, 1960).

In order to create the same lift as an airfoil of span $2b$, the bound vortex has to be a length $2a$, corresponding to the distance between tip vortices. Thus the total lift of an airfoil of span $2b$ is

$$L = 2a\rho\Gamma U. \quad (13)$$

It can be shown that the downward velocity (downwash) created by an airfoil is a constant along the span and is given by

$$w_d = \frac{\Gamma}{4b} \quad (14)$$

(Houghton & Brock, 1960). The result of applying the Kutta-Zhukovsky theorem to the downwash velocity, w_d , is a force in the opposite direction of the motion of the airfoil and is referred to as induced drag, D_I , (Figure 3)

$$D_I = 2a\rho\Gamma w_d. \quad (15)$$

The induce drag can also be written by substituting w_d from equation (14) to give

$$D_I = \frac{\pi}{8}\rho\Gamma^2. \quad (16)$$

A more common form of the induced drag equation (Equation 3) can be derived by substituting in the above equation for Γ from equation (13) to give

$$D_I = \frac{\pi}{8}\rho\left[\frac{L}{\rho\pi Ub/2}\right]^2 = \frac{L^2}{2\rho\pi b^2 U^2}. \quad (17)$$

In summary, then, it is possible to represent a wing by a vortex system forming three sides of a rectangle (Figure 4): along the y axis a vortex filament of strength Γ of length $2a$ represent the wing, and along the x axis two trailing vortices of the same strength as the bound vortex represent the trailing wake. The system of vortices can also be looked upon as a single long vortex bend in the shape of horseshoe.

Figure 3. Circulation (Γ) superimposed on forward velocity (U) and downwash (w_d) to produce lift (L) and induced drag (D_I) respectively (Houghton & Brock, 1960).

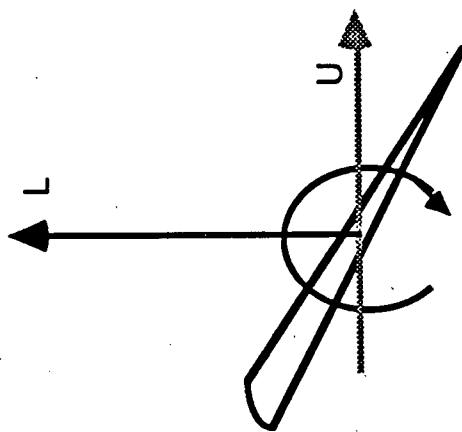
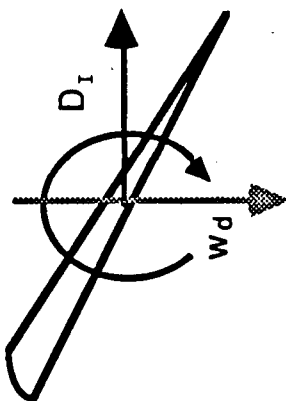
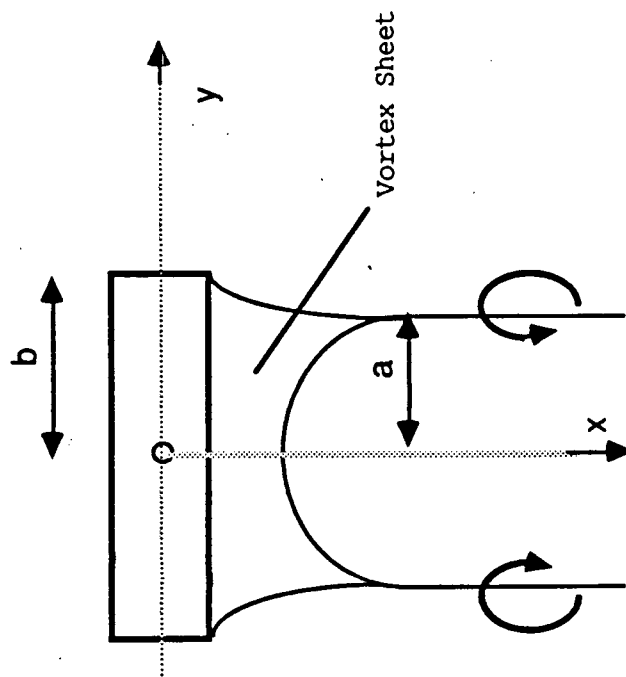
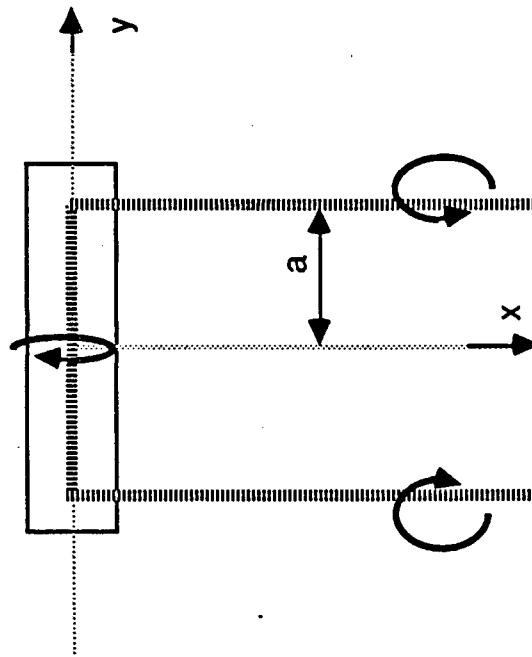


Figure 4. Wing with rolled-up vortex sheet (left) and its equivalent horseshoe vortex: bound vortex ($|||$) and tip vortex (\equiv).



Upwash Velocity Calculations

The vector velocity field induced by a line vortex in a shape of a horseshoe and strength Γ is calculated by applying the Biot-Savart law (McCormick, 1979). The vertical velocity component at a distance δx , δy away from center of the wing is

$$w(\delta x, \delta y) = -\frac{\Gamma}{4\pi} \frac{1}{\delta x} \left\{ \frac{\delta y + a}{\sqrt{\delta x^2 + (\delta y + a)^2}} - \frac{\delta y - a}{\sqrt{\delta x^2 + (\delta y - a)^2}} \right\} \\ - \frac{\Gamma}{4\pi} \frac{1}{(\delta y - a)} \left\{ 1 - \frac{\delta x}{\sqrt{\delta x^2 + (\delta y - a)^2}} \right\} \\ + \frac{\Gamma}{4\pi} \frac{1}{(\delta y + a)} \left\{ 1 - \frac{\delta x}{\sqrt{\delta x^2 + (\delta y + a)^2}} \right\} \quad (18)$$

(Milne-Thomson, 1958; Lugt, 1983).

Figure 5 shows the magnitude of the vertical velocity near a moving airfoil, with its center at the origin, and its tip at $y = \pm 1$. Updraft occurs in front and also in the outboard region of the tip vortices, located on the line $y = \pm \pi/4$. The downwash occurs behind the airfoil and between the two tip vortices. While the downwash is constant behind the airfoil, the upwash takes its maximum value at the tip vortex and then rapidly diminishes with increasing distance from the wing.

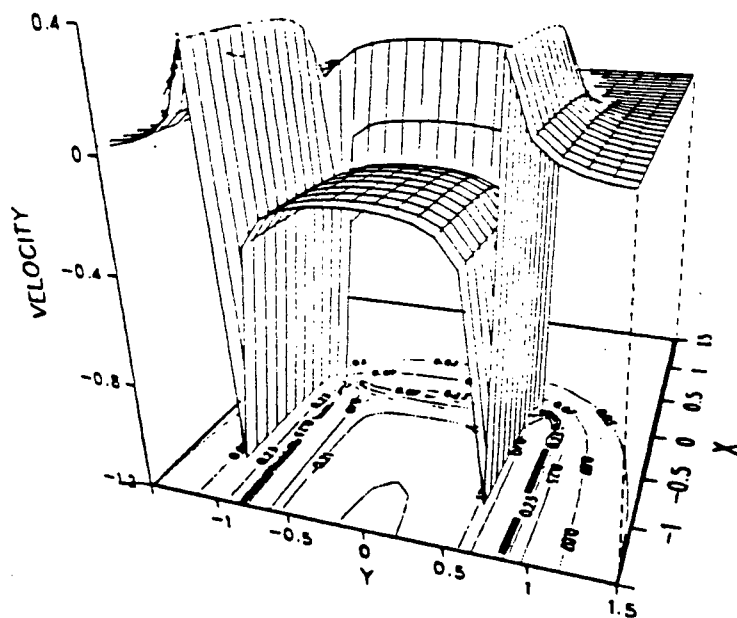
Induced Drag Reduction



Flying performance of a bird is influenced by the upwash created by other birds in the flock. The upwash brings about a decrease in the total induced drag of the flock. The extent of the reduction in induced drag depends on the wing-tip spacing and the number of birds in the flock. A general account of the influence of two birds flying in formation is given and then expanded to n birds.

An isolated wing produces a vertical velocity component, w_d , that is due to the wing's own vortex system. The upwash, w , is the vertical velocity induced by the vortex system of the second wing. Flying in the influence of each other results in a smaller downwash, $w_d + w$ (the sign of the downwash is always positive and

Figure 5. Vertical flow in the vicinity of a lifting wing, moving in the positive x direction. The wing tips are at points $x = 0$ and $y = \pm 1$.



the sign of the upwash is negative). The induced drag of the first wing, by analogy with equation (15), is

$$D_{I1} = 2a\rho\Gamma(w_d + w) \quad (19)$$

which can be written as

$$D_{I1} = 2a\rho\Gamma w_d + 2a\rho\Gamma w \quad (20)$$

$$D_{I1} = D_{I11} + D_{I12}. \quad (21)$$

The component D_{I11} is called the "self-induced drag" and D_{I12} is known as the "mutually induced drag" (Reid, 1932). In other words, D_{I11} denotes the self-induced drag of wing 1, while D_{I12} is the mutually induced drag experienced by wing 1 as a result of the vertical velocities induced by wing 2. The same argument can be made with the influence of the second wing on the first. The induced drag on the second wing is

$$D_{I2} = D_{I22} + D_{I21}. \quad (22)$$

The total induced drag of a flock containing 2 birds is

$$D_I(2) = D_{I11} + D_{I12} + D_{I22} + D_{I21}. \quad (23)$$

In general, the total induced drag of a flock with n birds (wings) is equal to the sum of the self-induced drags of its component wings plus as many mutually drags as there are permutations of its wings in pairs (Reid, 1932). Mathematically, the total induced drag of a flock of n birds is

$$D_I(n) = \sum_{i=1}^n \sum_{j=1}^n D_{Iij}. \quad (24)$$

The mutually induced drag for a pair of wings depends on the relative position of each wing. The greater the distance between the wings the smaller is the mutual induced drag. More accurately, the second term of equation (20) should be written as

$$D_{I12} = 2a\rho\Gamma w(\delta x, \delta y), \quad (25)$$

where wing 2, whose vortex influences the flow at wing 1, is located at the point $(\delta x, \delta y)$. Produced by wing 2, the upwash, $w(\delta x, \delta y)$, varies along the span of wing 1. Taking the integral mean value of the upwash over the span a of wing 1 gives

$$D_{I12} = 2a\rho\Gamma\bar{w} \quad (26)$$

(Hummel, 1983).

The average upwash velocity induced by a wing at a point $(\delta x, \delta y)$ is

$$\bar{w}(\delta x, \delta y) = \frac{1}{2a} \int_{\delta y-a}^{\delta y+a} w(\delta x, \eta) d\eta. \quad (27)$$

After substituting the result of the above integration into equation (26), the induced drag on a wing centered at $(\delta x, \delta y)$ (wing 1) due to the presence of a vortex system at the origin (wing 2) is given by

$$D_{I12} = \frac{\rho\Gamma^2}{4\pi} \left[\frac{1}{\delta x} \left\{ \sqrt{\delta x^2 + (\eta - a)^2} - \sqrt{\delta x^2 + (\eta + a)^2} \right\} - \left\{ \log(\eta - a) + \log \left(\frac{\delta x + \sqrt{\delta x^2 + (\eta - a)^2}}{(\eta - a)} \right) \right\} + \left\{ \log(\eta + a) + \log \left(\frac{\delta x + \sqrt{\delta x^2 + (\eta + a)^2}}{(\eta + a)} \right) \right\} \right] \Bigg|_{\eta=\delta y-a}^{\eta=\delta y+a} \quad (28)$$

(Moran, 1984). In the case of calculating the total induced drag of a flock, as opposed to the induced drag of each bird with respect to position in a flock, Munk's Stagger theorem is applied to simplify the calculations. The theorem states that "a collection of lifting surfaces (birds) may be translated in the streamwise direction (x -axis) without affecting the total induced drag of the system (flock) as long as the circulation of every wing (or lift) is unchanged" (Higdon and Corrsin, 1978). For example, a flock in line abreast formation will have the same total induced drag as one in V formation. Although, staggering in the x direction causes a redistribution of the induced drag for each bird, the total of the induced drag of the flock does not change. The consequence of this theorem is that the total induced drag of a flock depends on the scatter along the y -axis and not on the depth distribution

along the x -axis. Since the calculation of the total induced drag is independent of the x -axis, δx in equation (28) is set to zero, which is equivalent to saying that the flying formation is unstaggered. The mutually induced drag can now be simplified to

$$D_{I12} = \frac{\rho\Gamma^2}{4\pi} \left[\log \left(\frac{\eta + a}{\eta - a} \right) \right] \bigg|_{\eta=\delta y-a}^{\eta=\delta y+a} \quad (29)$$

which further reduces to

$$D_{I12} = \frac{\rho\Gamma^2}{4\pi} \log \left[1 - \left(\frac{2a}{\delta y} \right)^2 \right]. \quad (30)$$

In the case of unstaggered flight formation, it can be shown that the mutually induced drag terms between a pair of birds is equal. In other words,

$$D_{I12} = D_{I21} \quad (31)$$

(Reid, 1932; Prandtl & Tietjens, 1957).

Substituting $D_{I11} = \frac{\pi}{8}\rho\Gamma^2$ (equation (16)), into equation (30) gives

$$D_{I12} = \frac{2D_{I11}}{\pi^2} \log \left[1 - \left(\frac{2a}{\delta y} \right)^2 \right] \quad (32)$$

the mutually induced drag of a bird that is δy apart from the second bird.

In general, the distribution of n birds along the y -axis is a function of the wing-tip spacing s and the semi-wing span b (Figure 6). If the left most bird in a flock is numbered 1, and the next bird numbered 2 and so on to n , the distance between bird i and j is given by

$$\delta y_{ij} = |i - j|(2b + s). \quad (33)$$

Mutually induced drag of bird i due to presence of bird j can be written as

$$D_{Iij} = \frac{2D_{I11}}{\pi^2} \log \left[1 - \left(\frac{2a}{|i - j|(2b + s)} \right)^2 \right]. \quad (34)$$

By assuming that all birds are identical, in that they have the same wing span, aspect ratio, and weight, the problem of calculating the total induced drag (Equation (24)) reduces considerably. For instance, all terms such as D_{I11} , $D_{I22} \dots D_{Inn}$ are equal and can be replaced by $n \cdot D_{I11}$. Furthermore, the mutually induced drag terms in general can be written as

$$D_{Iij} = D_{Iji} \quad (35)$$

as a result of equation (31). Equivalently, equation (24) can now be written as

$$D_I(n) = nD_{I11} + 2 \sum_{i=1}^{n-1} \sum_{j=i+1}^n D_{Iij}. \quad (36)$$

Substituting equation (34) for D_{Iij} , equation (36) can be written as

$$D_I(n) = nD_{I11} + \frac{4D_{I11}}{\pi^2} \sum_{i=1}^{n-1} \sum_{j=i+1}^n \log \left[1 - \left(\frac{2a}{|i-j|(2b+s)} \right)^2 \right] \quad (37)$$

for n birds in a flock.

In a flock of size n , the induced drag on a single bird, $\bar{D}_I(n)$, is equal to the total induced drag of the flock divided by its size. That is

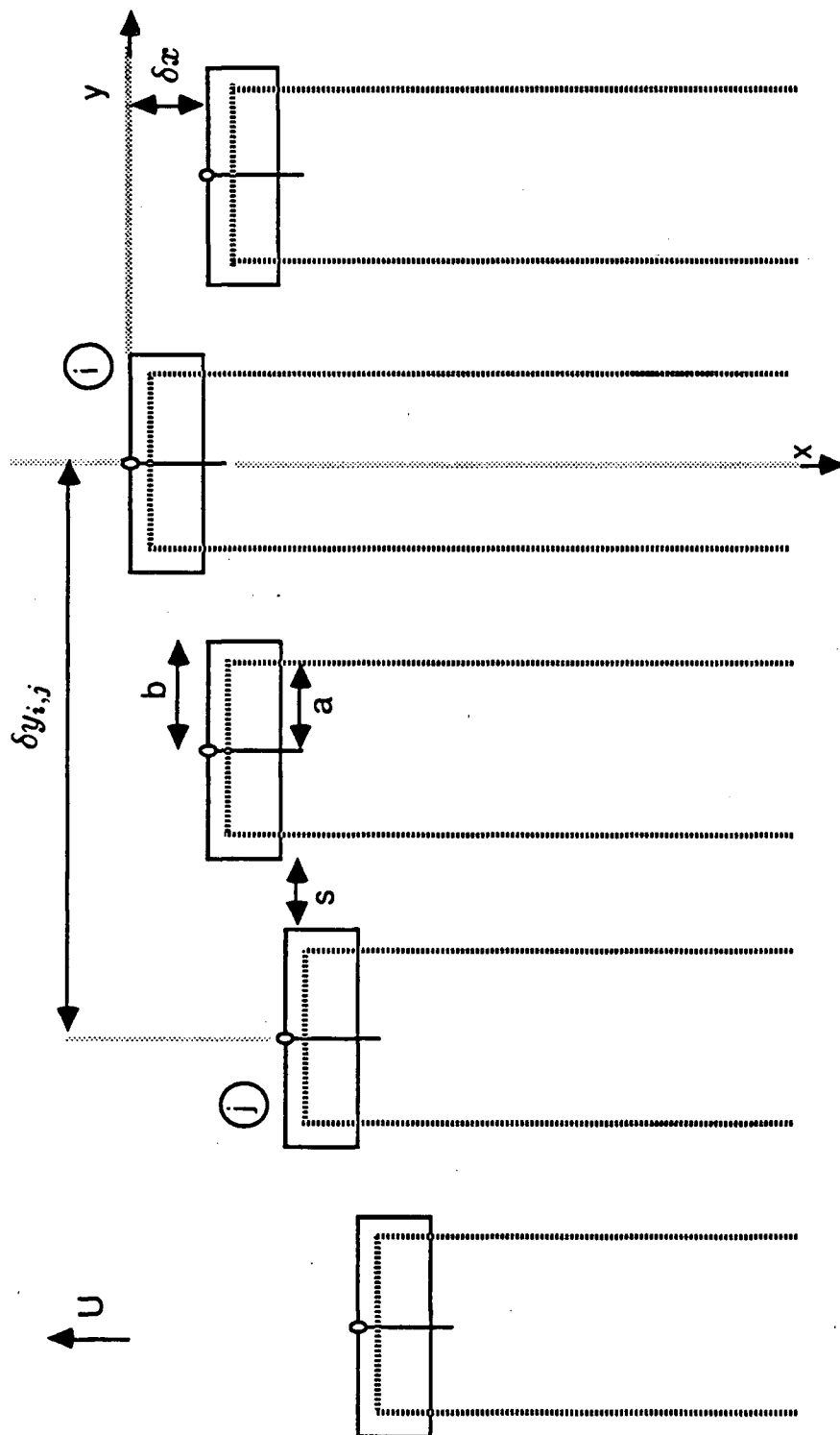
$$\bar{D}_I(n) = \frac{D_I(n)}{n}. \quad (38)$$

Substituting equation (37) for $D_I(n)$ in equation (38), and noting that D_{I11} and D_I are notationally equivalent, the above equation can be written as

$$\bar{D}_I(n) = \underbrace{D_I}_{\text{Solo term}} + \frac{4D_I}{\pi^2} \frac{1}{n} \sum_{i=1}^{n-1} \sum_{j=i+1}^n \underbrace{\log \left[1 - \left(\frac{2a}{|i-j|(2b+s)} \right)^2 \right]}_{\text{Flock-associated terms}}. \quad (39)$$

Essentially, the above equation has the following meaning. The first term, D_I , represents the induced drag experienced if a bird was to fly solo. The second term is the flock associated reduction in induced drag as a result of flying in the upwash

Figure 6. Distribution of $n = 5$ birds and their horseshoe vortex on the x - y plane. Starting from the left, each bird is numbered from 1 to n . The distance, as projected on the y -axis, between bird number i and j is $\delta y_{ij} = |i - j|(2b + s)$, where b is the semi-wing span and s is the distance between adjacent birds perpendicular to the flight path. Each bird is of span $2b$, represented by a bound vortex of length $2a$, where $a = \pi/4b$.



* field created by the other $n - 1$ birds. Flock-associated reduction is negative. As a result, the induced drag for a member of the flock is less than what would be experienced if flying solo. Only if the formation is such that each bird flies in the flight path of other (in the downwash region, see Figure 5) results in the induced drag being higher than that for a single bird.

The extent of reduction of induced drag by formation flight is dependent on wing-tip spacing, s , the distance between wing-tips of adjacent birds perpendicular to the flight path and flock size, n . Since the region of the upwash occurs inboard of the actual wing-tips, certain overlap of the wing-tips may occur (Figure 5). In this case the wing-tip spacing, s , is negative. The ratio $\bar{D}_I(n)/D_I$ is used to assess the benefit of formation flight vs solo flight. A small ratio implies large savings in formation flight. When the ratio is equal to one, both formation and solo flight, in terms of induced drag, are equivalent. As the wing-tip spacing as percent of the semi-wing span increases for a fixed flock size, say 20 birds, the ratio approaches one (Figure 7). Thus a flock with very large wing-tip spacing benefits less than a flock that flies in tighter formation. The benefit of formation flight increases with flock size; however, there is a limiting value as $n \rightarrow \infty$ (Lissaman & Schollenberger, 1976). The induced drag of a single bird in a flock as n becomes indefinitely large is given by

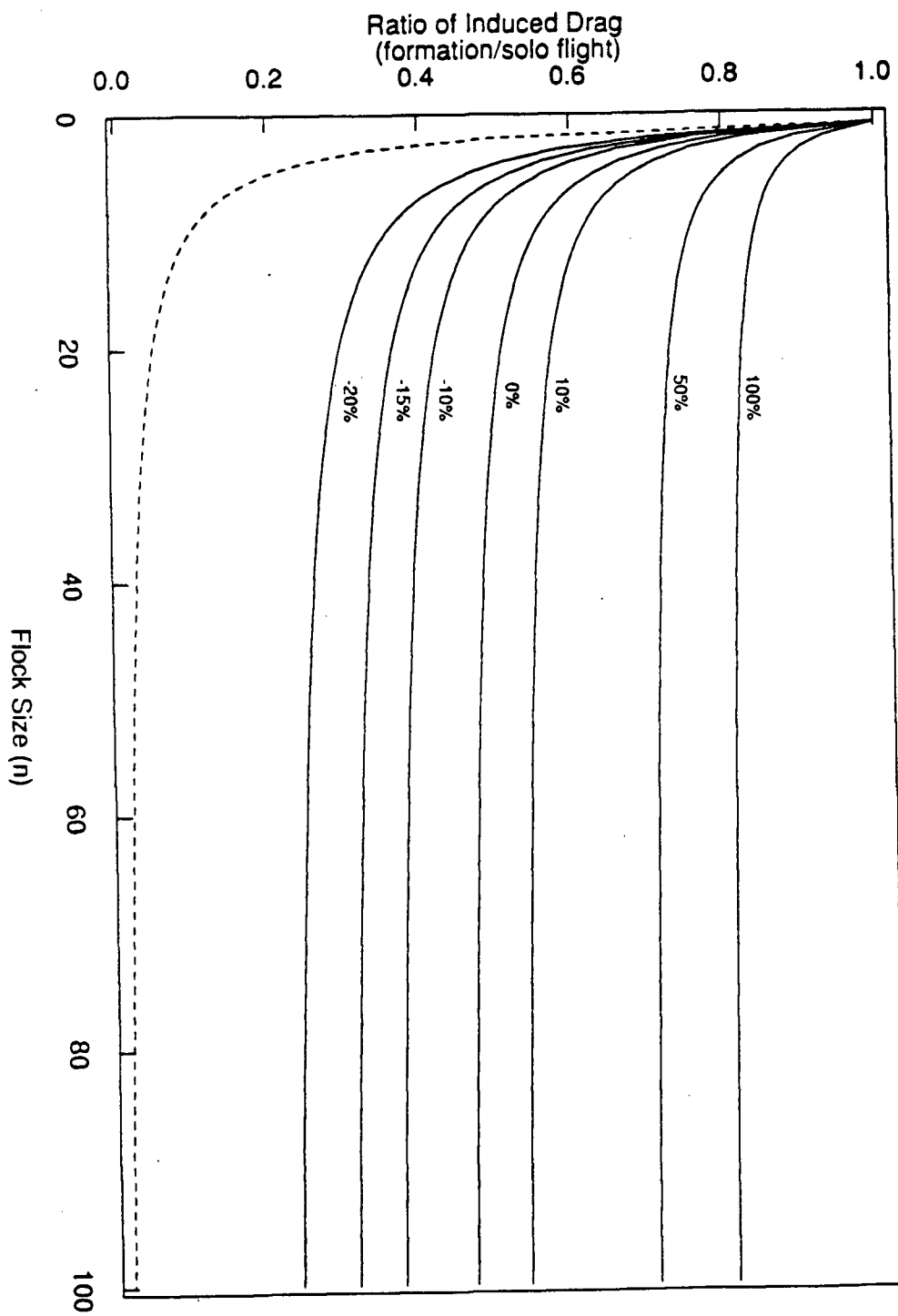
$$\lim_{n \rightarrow \infty} \bar{D}_I(n) = D_I + \frac{4D_I}{\pi^2} \log \left[\frac{\sin(2a\pi/(2b + s))}{2a\pi/(2b + s)} \right] \quad (40)$$

(see appendix A for derivation).

Approximation Formula

In its current form, equation (39) is computationally intensive and mathematically awkward. To calculate the induced drag of a bird in a flock of size n requires at least $n^2/2$ operations. For instance, a flock of size $n = 100$ requires at least $10^4/2$ operations to calculate the induced drag. There are two main advantages of the approximation formula. Firstly, it is computationally less time-consuming, since

Figure 7. Ratio of induced drag in formation to solo flight, as a function of flock size, n , and various wing-tip spacing, s , as a percent of the semi-wing span (solid). Curves are shown for $s/b = +100, +50, +10, 0, -10, -15$, and -20% . For the special case when the wing-tip spacing is such that the tip vortices of the two adjacent birds overlap ($s = 2(a - b)$) the ratio is given by the dash line.



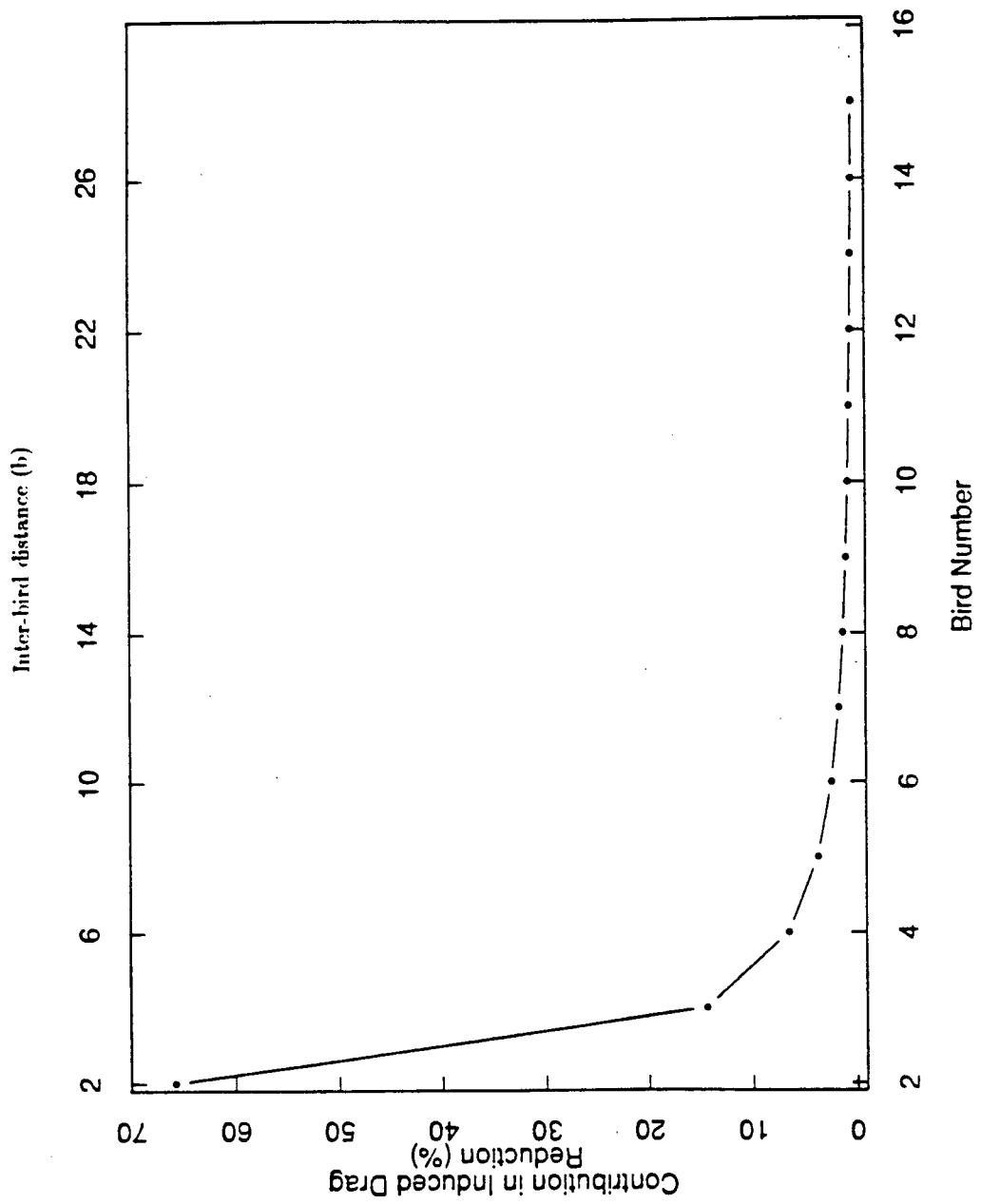
there are considerably less operations. Secondly, it provides a basis for generalization. The goal of the approximation technique is to eliminate the summation series in equation (39) and replace it with an analytic function.

There are basically two ways to reduce the number of operations in a formula containing a summation series. The first method is to truncate the series at some arbitrary term and discard the rest of the terms in the series. As a result of this method, the calculated value from the truncated series underestimates the true value. The second method is to assume that there is an indefinite number of terms in the series. In other words, the original series is assumed to be an infinite series. This method often leads to representation of the infinite series by an analytic function. The degree of overestimation depends on the contribution of the extra terms to the sum.

As the distance between a pair of birds gets large, the corresponding flock-associated term, in equation (39), gets small. To illustrate, in a flock of 15 birds, the percent contribution by the other birds to the total induced drag reduction of the left most bird (Bird 1) is shown in figure 8. In the case of flying abreast, with a wing-tip spacing of zero ($s = 0$) and semi-wing span of one ($b = 1$), the closest bird to Bird 1 contributes 65% of the entire induced drag reduction. For other birds, percent contribution drops off as the distance from them to Bird 1 increases. Incidentally, the smallest contribution to the entire induced drag reduction is by the 15th bird, furthest from Bird 1. It follows, then, that the addition of extra birds right of the 15th bird, in this case, will not greatly affect the total drag reduction of Bird 1.

The basis of the approximation technique is to assume that in a flock of size n there is an indefinite number of birds creating an upwash field when in reality there are only $n - 1$ birds. Figure 9 gives a pictorial representation of the approximation technique. Specifically, in a formation of n birds, the left and right most birds are assumed to be flanked to either starboard or port respectively, by an infinite

Figure 8. Percent contribution to the total induced drag reduction of the left most bird (Bird 1) by the neighboring birds numbered 2 through 15 (bottom x -axis), flying in abreast formation with a wing-tip spacing equal to zero ($s = 0$). The top axis is the distance of each bird as measured from Bird 1. Each bird is assumed to be of unit semi-span ($b = 1$).



number of birds (Figure 9(A & C)). However, the remaining birds, each having adjacent birds on either side, are assumed to be flanked on the left by an infinite number of birds and on the right by an infinite number of birds (Figure 9(B)). Following the above assumptions, the induced drag reduction on a bird in a flock of size n can be approximated by


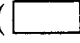

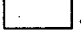
$$\bar{D}_I(n) \approx D_I + \frac{4D_I}{\pi^2} \frac{(n-1)}{n} \log \left[\frac{\sin(2a\pi/(2b+s))}{2a\pi/(2b+s)} \right] \quad (41)$$

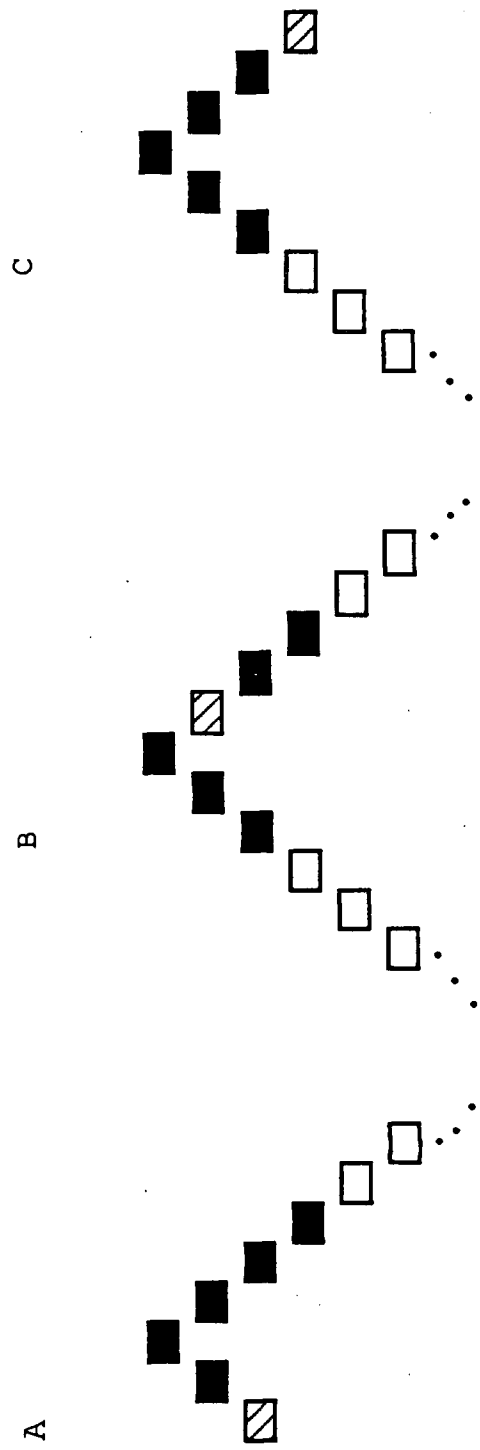
(see appendix B for detail). In the above form, the estimation of induced drag on a bird in formation flight is greatly simplified.

To test the accuracy of this method, the true value as calculated from equation (39), is compared to the value from the above approximation equation. The degree of accuracy is measured by the relative error, defined as

$$\text{Relative Error} = \left| \frac{\text{true} - \text{approximated}}{\text{true}} \right| \quad (42)$$

(Taylor, 1982). The relative error incurred by this approximation technique is plotted in figure 10. Evidently, the approximation formula is quite accurate for a specific range of wing-tip spacing and of flock size. Relative error is the largest for formations with small wing-tip spacing relative to the semi-wing span (s/b). In such tight formation, the updraft created by each bird contributes a significant amount of reduction in induced drag on any other bird in a flock. Not surprisingly, in a case where each bird has a significant effect, the introduction of an indefinite number of birds to a flock results in large overestimation of the drag reduction; consequently, the relative error for this case is large. The approximation formula for wing-tip spacing relative to semi-wing span of -20% guarantees the relative error to be less than 23% . However, as the wing-tip spacing increases, the relative error drops quickly. Figure 10, also, shows that the accuracy of the approximation formula increases with flock size. For example, the relative error drops from 12 to 5% for a flock size of 3 and 100 birds, respectively, at zero wing-tip spacing. As the

Figure 9. Pictorial representation of the approximation technique for $n = 6$ birds, solid plus one diagonal filled wing. (A & C) The left and right most birds in the vee formation () are assumed to be flanked on the opposite leg by an infinite number of birds (...). (B) Each bird inside a flock, for example , is assumed to be flanked by an infinite number of birds on both legs of the vee (...).



flock size increases the assumption of indefinite number of birds in a flock becomes truer; correspondingly, the relative error becomes smaller.

Another test for validity is to compare the calculated result of Lissaman and Schollenberger (1970, Figure 2) with the above approximation formula. In this case, the same order of magnitude of drag reduction turns out as calculated by Lissaman and Schollenberger. In other respects the behaviour of the estimate formula is similar to the family of curves they obtain. In particular, significant drag saving occurs at small wing-tip spacing; and the magnitude of the saving for a formation of 25 or more birds is nearly the same as for an infinite number of birds (Figure 11).

It should be remarked that equation (39) and consequently equation (41) has a singularity at wing-tip spacing $s = 2(a - b)$, where $a = \frac{\pi}{4}b$. In other words, the value of the function becomes infinite at the point $s = 2(a - b)$. Physically, this wing-tip spacing corresponds to when the tip vortices of adjacent birds overlap. Of interest is the total induced drag of a flock in such a flight formation.

Before generalizing for n birds, an account of the influence of two birds flying in formation for this case is given. Figure 12 shows the air flow due to the interaction between the two wings at such a spacing. As done previously, each wing in the flock is replaced by an equivalent horseshoe vortex. For a single wing of semi-span b , the bound vortex is of length $2a$; and the distance between the two counter rotating tip vortices is $2a$ (Figure 12 (A)). Due to its position, the lead bird's tip vortex, rotating clockwise, cancels the tip vortex, rotating anti-clockwise, of the second bird. The resulting flow is another larger horseshoe vortex. The bound vortex is now of length $4a$ and the distance between the tip vortices is also $4a$. Equivalently, the resulting vortex system can be generated by a single wing of semi-span $2b$ (Figure 12 (B)). This follows from the relation that $a = \frac{\pi}{4}b$. If a , as in this case, is doubled, then b is increased by the same amount. Thus the air flow of two birds, each of semi-span b , in this formation is equivalent to the flow produced by a single wing of semi-span

Figure 10. Effect of flock size and spacing ratio, s/b , on relative error as result of the approximation technique. Curves are shown for $s/b = -20, -15, -10, 0, +10, +50$, and $+100\%$.

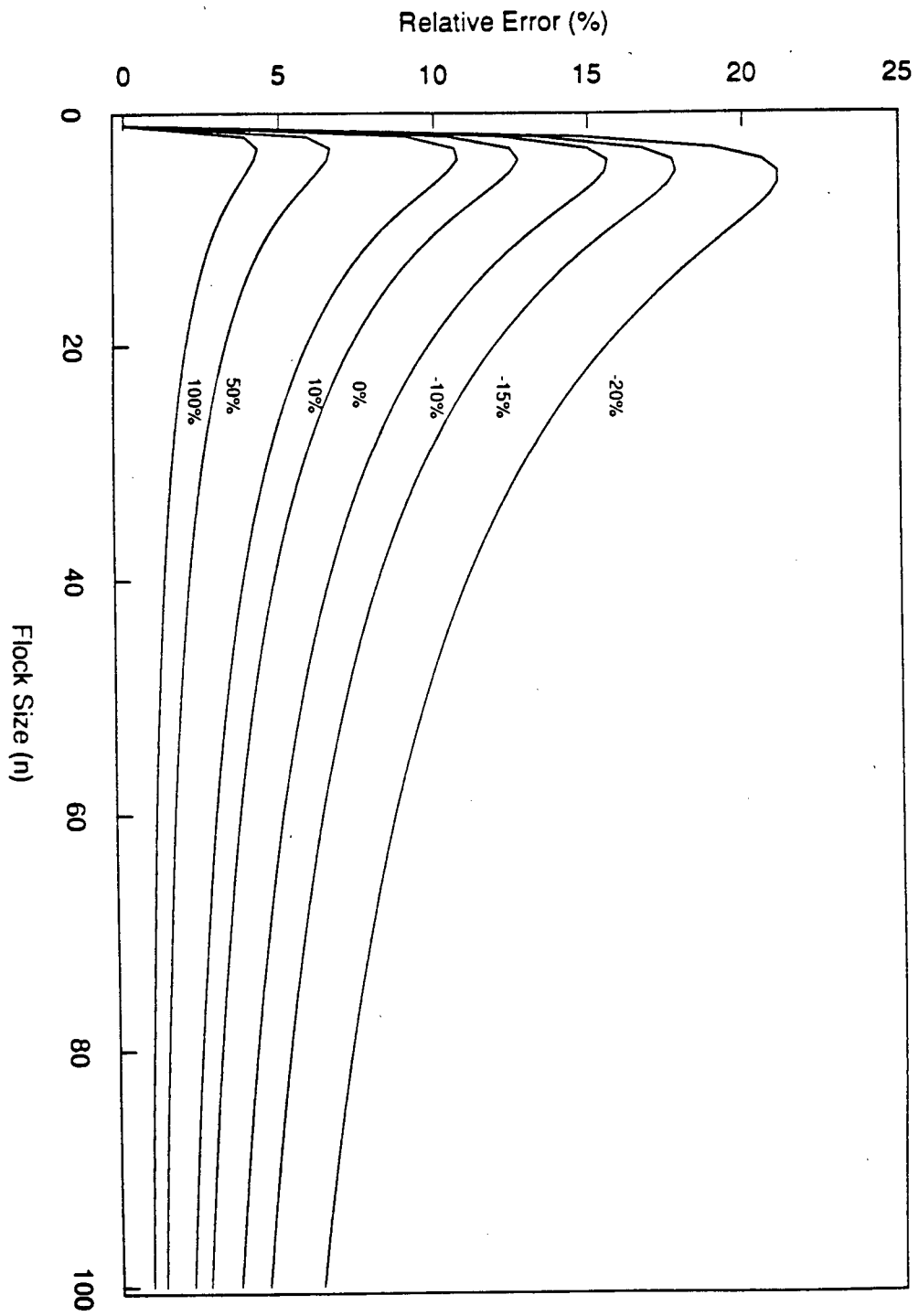
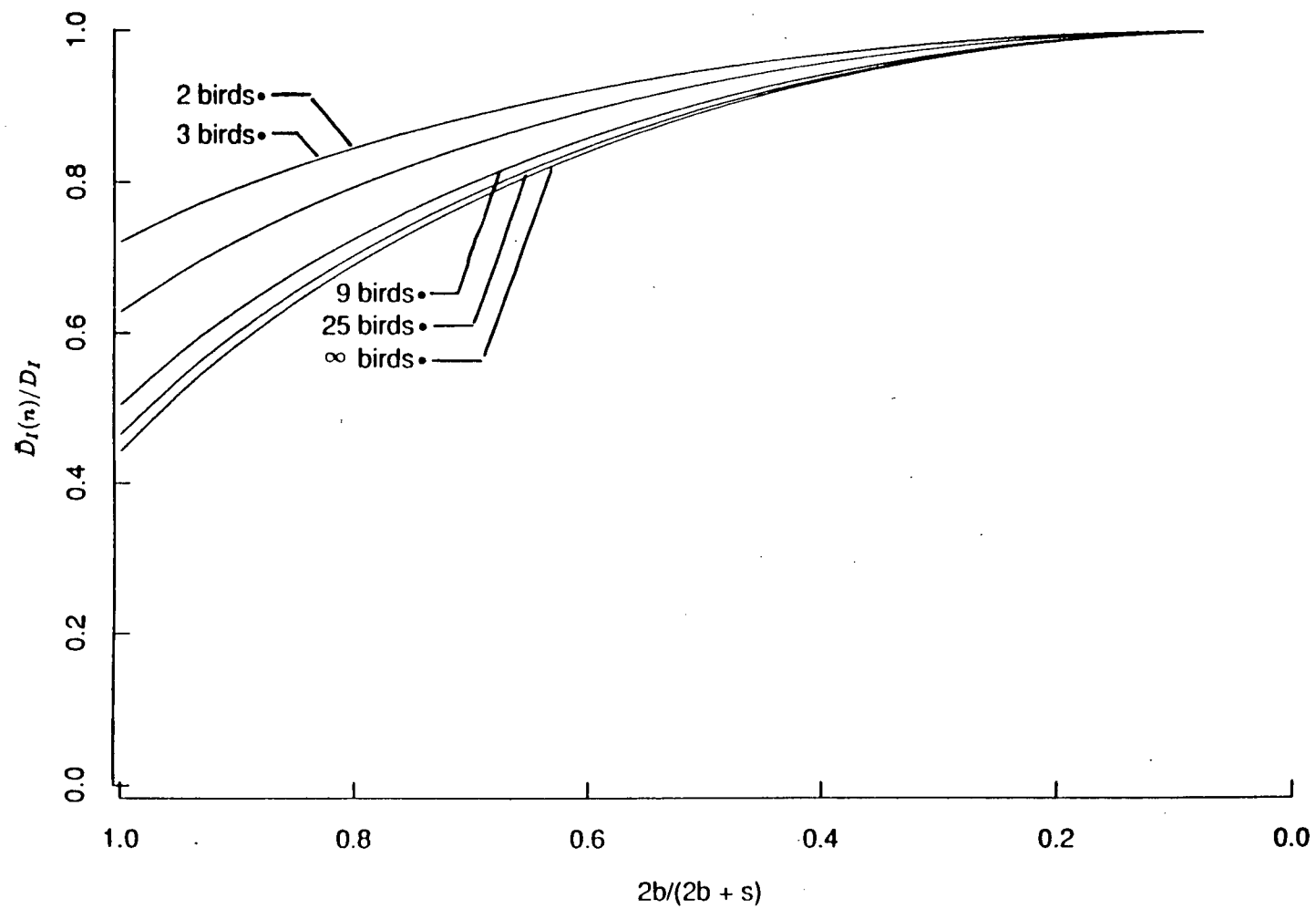


Figure 11. Induced drag in formation flight, $\bar{D}_I(n)$, relative to that in solo flight, D_I , for $n = 2, 3, 9, 25$ and infinite number of birds.



2b. As a result, the induced drag equation of a single wing (Equation 3) can be used to calculate the total induced drag of a flock. In particular, substituting b for $2b$ and L for $2L$ in equation (3) gives the total induced drag of a flock containing two birds

$$D_I(2) = \frac{(2L)^2}{2\pi\rho U^2(2b)^2} = \frac{L^2}{2\pi\rho U^2 b^2} = D_I. \quad (43)$$

Accordingly, the induced drag for a single bird in this case is

$$\bar{D}(2) = \frac{D_I}{2}. \quad (44)$$

In other words, the induced drag of a bird in a flock of size 2 is half the induced drag if the bird was to fly solo (D_I).

In general, the total induced drag for n birds can be calculated by substituting the lift L to be the total lift of all n birds, that is $n \cdot L$ and by substituting the semi-wing span b to be the total semi-span of all n birds, that is $n \cdot b$ into the induced drag equation for a single wing. Making the above substitutions into equation (3) gives the total induced drag of a flock of size n

$$D_I(n) = D_I. \quad (45)$$

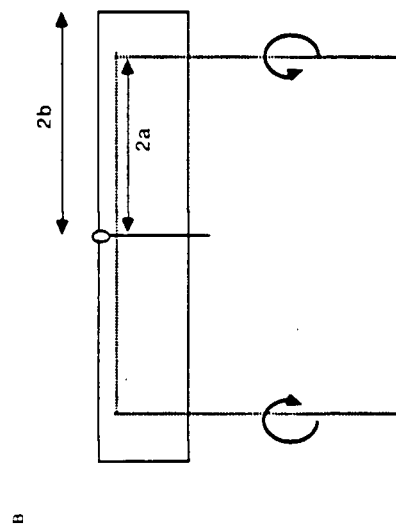
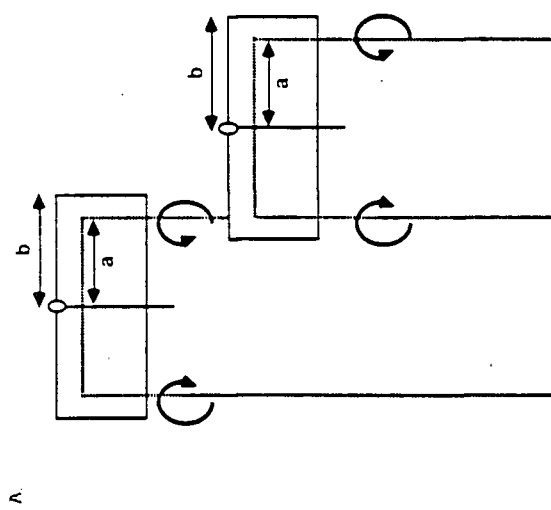
For any single bird in a flock of size n , the induced drag is

$$\bar{D}_I(n) = \frac{D_I}{n}. \quad (46)$$

Thus in a formation when the tip vortices of adjacent birds overlap, the induced drag of a single bird in a flock of size n is $1/n$ th the induced drag if it was to fly solo. Of all possible wing-tip spacing, maximum reduction in induced drag, as demonstrated by the dashed line of figure 7, occurs at wing tip spacing $s = 2(a - b)$, corresponding to when the tip vortices overlap.

In summary, within a range of wing-tip spacings the approximation formula (Equation (41)) is quite an accurate measure of induced drag for a member of a flock. Due to the nature of the approximation equation, flight formations where

Figure 12. Air flow pattern, as represented by a horseshoe vortex, of two wings each of semi-span b , located at wing-tip spacing $s = 2(a - b)$. Due to the positioning, tip vortex of the lead bird cancels the tip vortex of the second bird (A). The resulting flow, as shown by the horseshoe vortex in (B), is equivalent to a flow created by a single wing of span $2b$.



the wing-tip spacing $s = 2(a - b)$ equation (46) should be used. Interestingly, both formulas show that the induced drag of a bird in a flock is inversely related to flock size. This result greatly simplifies flight energetic calculations of a bird in different sized flocks.

Model

In formulating an optimal behaviour model three details are often considered: (1) choosing a currency (2) choosing an appropriate cost-benefit function with the appropriate constraints and (3) solving for the optimum (Pyke *et al*, 1977; Schoener, 1971). The currency in this case is energy, the cost-benefit function is net energy gained per unit energy expended, and the optimum is the flock size which maximizes the cost-benefit function, subject to various constraints. Here, energy gain (E_{in}) and energy expenditure (E_{out}) are the result of foraging and flying, respectively.

Energy Expenditure (flying cost)

Analogous to solo flight cost equation 8, energy expenditure for a bird in formation flight is given by

$$E_{out} = (D_P + \bar{D}_I(n))d. \quad (47)$$

In formation flight, the sum of profile and parasite drag is the same as for a solo bird, D_P , whereas the induced drag, $\bar{D}_I(n)$, is reduced, and it is now a function of wing-tip spacing, and flock size. As shown previously, induced drag can be expressed by two approximation formulas, depending on the choice of wing-tip spacing. The result of substituting equation (41) for $\bar{D}_I(n)$ is shown in appendix C. The case when the wing-tip spacing causes the tip vortices to overlap is considered here. In such formation $\bar{D}_I(n) = D_I/n$; accordingly, the flight cost equals

$$E_{out} = (D_P + \frac{D_I}{n})d. \quad (48)$$

Substituting equation (2) and (3) for D_P and D_I respectively, and grouping terms gives the energy expenditure of a bird in a flock of size n flying at a speed U for a distance d

$$E_{out} = (k_p U^2 + \frac{k_i}{n} U^{-2})d. \quad (49)$$

The maximum range speed, which minimizes flying cost per unit distance travelled, is given by solving the equation

$$\frac{d}{du} \left[\frac{E_{out}}{d} \right] = 2k_p U - \frac{2k_i}{n} U^{-3} = 0. \quad (50)$$

Solving for U gives the maximum range speed of the flock

$$U_{mr}(n) = \left[\frac{k_i}{k_p} \frac{1}{n} \right]^{1/4}. \quad (51)$$

Equation (51) shows that with increasing flock size cruising speed of the flock decreases. Relative to the optimum speed of a solo flyer, $U_{mr} = (k_i/k_p)^{1/4}$, the maximum range speed of the flock decreases as $n^{-1/4}$. Due to a lower cruising speed, birds in a larger flock will take a longer time to travel the same distance than birds in a smaller flock. In effect, the airborne time t_a during a migration leg of distance d is

$$t_a = \frac{d}{U_{mr}(n)} = d \left[\frac{k_p}{k_i} \right]^{1/4} n^{1/4}. \quad (52)$$

Finally, substituting equation (51) for U in equation (49) gives the flying cost of a bird in a flock of size n , travelling a distance d at the maximum range speed

$$E_{out} = 2\sqrt{k_p \cdot k_i} \frac{d}{\sqrt{n}}. \quad (53)$$

Equation (53) shows that flying cost for an individual decreases as the number of birds increases in the formation. More specifically, this cost decreases as $n^{-1/2}$.

Energy Gain (feeding)

It is assumed that birds do not feed during their journey and so any energy gain occurs only at a foraging site. The total energetic gain, E_{in} , will equal the rate of prey encountered times the time spent foraging. Assuming that an individual forager captures food according to a Poisson process with parameter λ (number of

prey (net energy equivalent) per unit time) (Mangel & Clark, 1988), then the net energy gain for a patch residence time, t_p , is

$$E_{in} = \lambda \cdot t_p. \quad (54)$$

The total time spent flying and foraging, T , is given by

$$T = t_p + t_a. \quad (55)$$

Substituting for t_p into equation (54) gives

$$E_{in} = \lambda(T - t_a). \quad (56)$$

Equation (56) shows that as the airborne time increases the total energy gain decreases. Substituting for t_a (Equation (52)) in equation (56) gives

$$E_{in} = \lambda(T - d \left[\frac{k_p}{k_i} \right]^{1/4} n^{1/4}). \quad (57)$$

In effect, net energy gain for an individual decreases with increasing flock size.

Ratio of Energy Gain to Energy Expenditure

Let the ratio of net energy gain/energy expenditure be

$$R = \frac{E_{in}}{E_{out}} \quad (58)$$

(Pyke *et al*, 1977; Schmid-Hempel *et al*, 1985). Substituting equations (53) and (57), into the above ratio gives

$$R(n) = \frac{\lambda \sqrt{n} (T - d \left[\frac{k_p}{k_i} \right]^{1/4} n^{1/4})}{2d \sqrt{k_p \cdot k_i}}. \quad (59)$$

The above equation is maximized when $dR(n)/dn = 0$. So, $R(n)$ is maximized when,

$$\frac{\lambda}{2d \sqrt{k_i \cdot k_p}} \left(\frac{1}{2} T n^{-1/2} - \frac{3}{4} d \left[\frac{k_p}{k_i} \right]^{1/4} n^{-1/4} \right) = 0. \quad (60)$$

Solving the above equation gives n_{opt} , a value of n that maximizes equation (59),

$$n_{opt} = \frac{16}{81} \frac{k_i}{k_p} \left[\frac{T}{d} \right]^4. \quad (61)$$

Finally, substituting $U_{mr} = (k_i/k_p)^{1/4}$ (Equation (10)) into the above equation gives

$$n_{opt} = \frac{16}{81} U_{mr}^4 \left[\frac{T}{d} \right]^4, \quad (62)$$

where U_{mr} is the maximum range speed for a solo bird.

For completeness, it can be shown that equation (59) is a maximum at $n = n_{opt}$, for at this value the second derivative of the function is negative; in particular,

$$\left. \frac{d^2 R(n)}{dn^2} \right|_{n=n_{opt}} = -\frac{729}{1024} \lambda \frac{k_i}{k_p^2} \left[\frac{d}{T} \right]^5 < 0. \quad (63)$$

Results

Conditions for Solo Flight

The model makes predictions on the optimum number of birds in a flock. Provided that the value of d , U_{mr} , and T are known a corresponding flock size can be calculated. Here, however, value of d , U_{mr} and T that yield a flock size of one (solo flight) is examined. In other words, n_{opt} is set equal to one in equation (62):

$$d = \frac{2}{3}U_{mr}T. \quad (64)$$

The conditions for solo flight depends on the value d , U_{mr} , T such that the above equality holds. For instance, in figure 13, for a given U_{mr} , a solid line divides the value of d and T pairs that predict solo flight (below the line) from the pairs that predict optimum flock size greater than one (above the line). Furthermore, figure 13 shows that as the value of U_{mr} increase the region for solo flight (below the line) also increases. Thus birds with large U_{mr} are more likely to fly solo than birds with low U_{mr} .

Moreover, the condition for solo flight can also be expressed as a ratio of two time variables. Substituting $d = U_{mr} \cdot t_a$ into equation (64) gives

$$\frac{T}{t_a} = \frac{3}{2} \quad (65)$$

which can be also expressed as

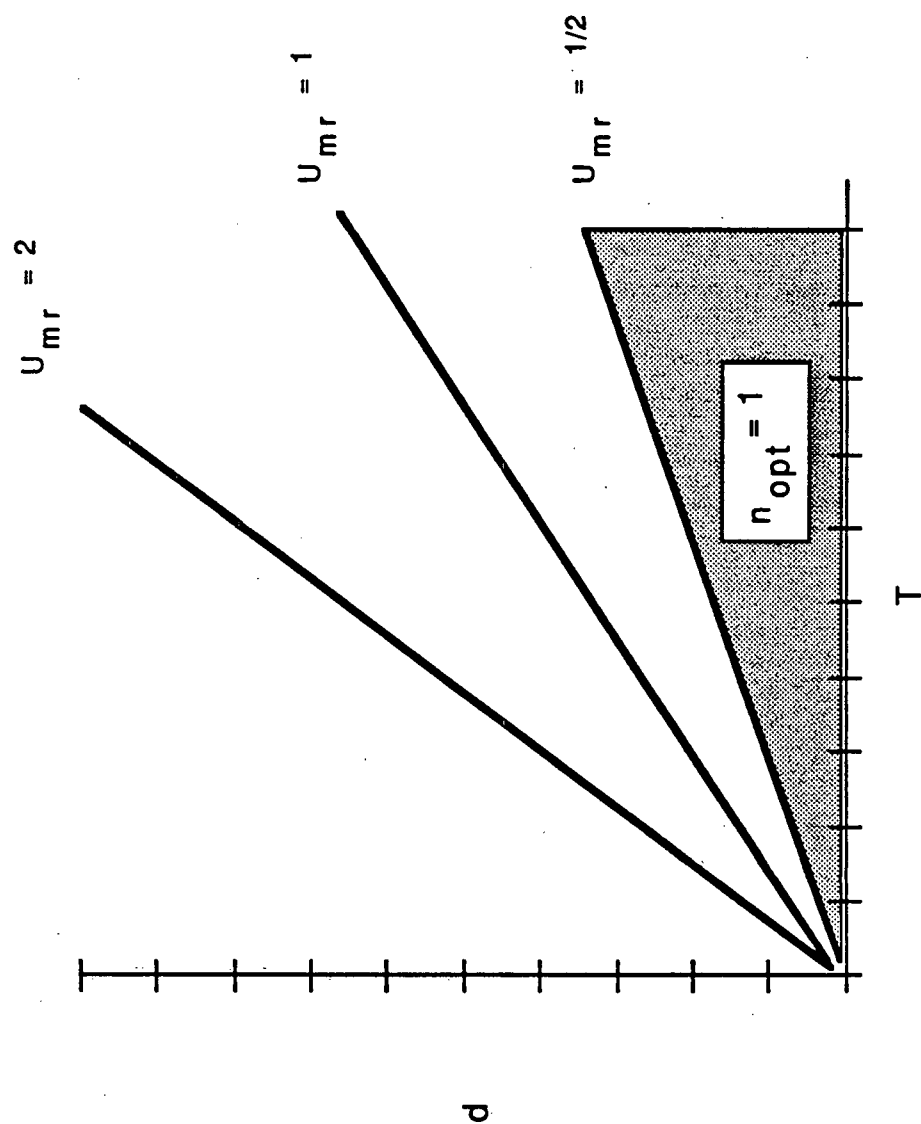
$$\frac{T}{t_a} = \frac{t_a + t_p}{t_a} = \frac{3}{2}. \quad (66)$$

Thus the condition for solo flight is when

$$\frac{t_p}{t_a} = \frac{1}{2}. \quad (67)$$

In other words, under the conditions where time spent feeding is one half the flight time birds should fly solo.

Figure 13. Condition for solo flight depends on the value of d , U_{mr} and T . For a given U_{mr} , a solid line divides the values of d and T pairs that predict solo flight (below the line) from d and T pairs that predict optimum flock size greater than one (above the line). To illustrate, say $U_{mr} = 1/2$, (T, d) pairs that fall in the grey region correspond to solo flight while pairs that fall in the white region correspond to formation flight.



Optimum Flock Size and Wing-tip Spacing

Birds in a flock have a choice of whether to fly in tight or loose formation. A tight formation is when the wing-tip spacing is small or, when the wing tips overlap, negative. As was shown in figure 7, maximum induced drag reduction occurs when the wing-tip spacing is such that the tip vortices of adjacent bird cancel each other out. The corresponding optimum flock size for such a spacing is given by equation (62). However, for other spacings, the optimum flock size is given by

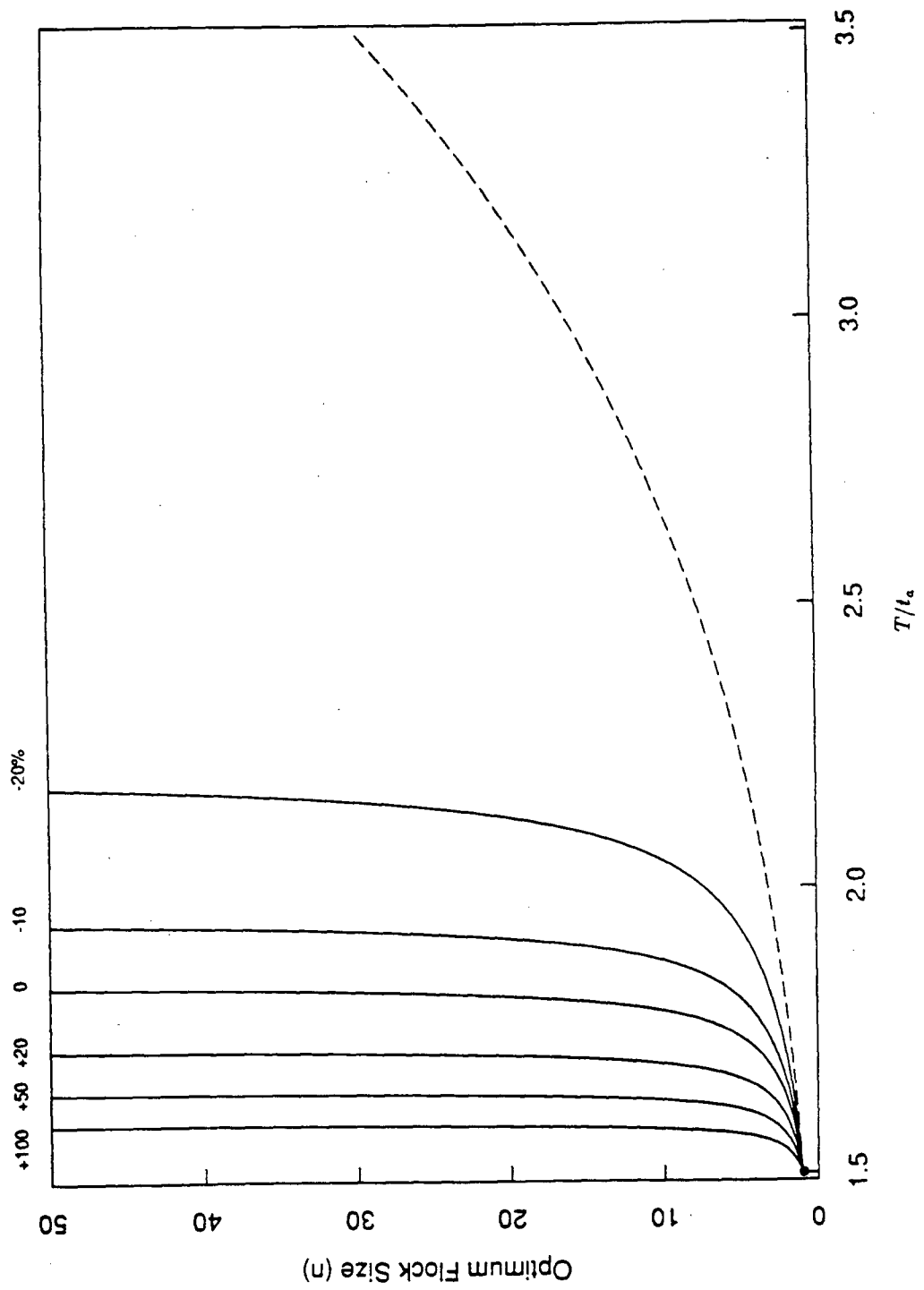
$$n_{opt}(s) = \frac{A}{1/n_{opt} - B} \quad (68)$$

where both A and B are a function of wing tip spacing, s (see appendix C , Equations C3 & C4). As shown in figure 14, for the same value of T/t_a , the smallest optimum flock size results when the wing-tip spacing gives the maximum drag reduction (dash line). As the wing-tip separation relative to the semi-wing span (s/b) increases the predicted number of birds in a flock also increases. To compensate for a lower induced drag reduction which occurs at large wing-tip spacing the number of birds in a flock is increased. Finally, figure 14 shows that for any wing-tip spacing, as the ratio of T/t_a increases so does the predicted optimum flock size.

Optimum vs Maximum Flock Size

Although the model predicts an optimum number of birds in a flock, an examination of the cost-benefit function (Equation (59)) shows that a flock may form which exceeds the optimum size (Sibly, 1983). Figure 15 shows that the curve specifying individual efficiency, R , as function of flock size is concave downward and has a peak at n_{opt} , the size yielding maximum efficiency. Due to the downward concavity of the curve, individual efficiency decreases in the region where flock size is larger than n_{opt} . Specifically, at a flock size n_* , the curve is at the same level as that for a solo flyer. Accordingly, individual birds in a flock of size n_* will experience the same benefit as a solo bird. By forming flocks larger than n_* results in

Figure 14. Optimum flock size is plotted against T/t_a . Curves correspond to wing-tip spacing, expressed by a non-dimensional ratio, s/b (+100, +50, +20, 0, -10, -20%). Smallest flock size occurs at wing-tip spacing $s = 2(a - b)$ (dash line), flock configuration for maximum induced drag reduction.



benefits smaller than that of flying solo. Thus, it follows that the maximum flock size is n_* . Mathematically, the maximum flock size, n_* , satisfies

$$R(1) = R(n_*). \quad (69)$$

Grouping terms (see Appendix D), the following relation can be derived between n_{opt} and n_*

$$n_{opt} = \frac{16}{81} \left[\frac{n_*^{3/4} - 1}{n_*^{1/2} - 1} \right]^4. \quad (70)$$

While not directly solving for n_* , it is shown in appendix D that the upper bound of n_* is be given by

$$n_* < \frac{81}{16} n_{opt} \approx 5 \cdot n_{opt}. \quad (71)$$

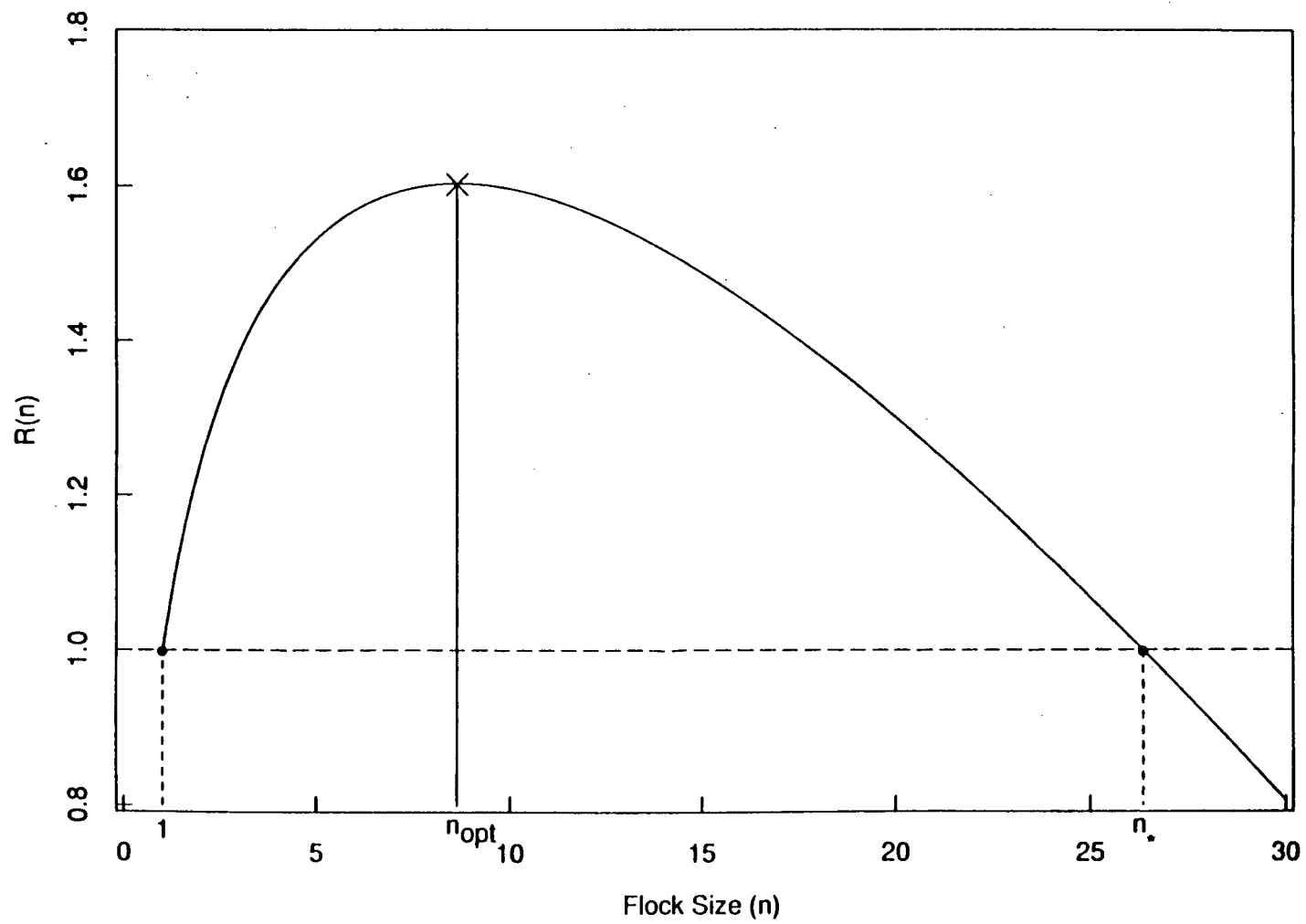
Thus the maximum flock size is no greater than five times the predicted optimum flock size. When a flock size exceeds $5 \cdot n_{opt}$ birds, the benefit of solo flight outweigh that of group flight.

Due to decreasing benefit, as the number of birds increases beyond the optimum size, a large flock may become unstable. For example, a flock will continue to attract individuals until the benefit of group flight equals that of solo flight. For this reason no other bird will join a flock that contains the maximum number of birds, n_* . However, compared to a large single flock, a greater benefit can be achieved by breaking up in to smaller flocks, each of size approximately equal to n_{opt} . Hence, breaking up of a flock is highly likely once its size has surpassed the optimum number.

Effect of U_{mr} on Optimum Flock Size

Estimates can be made of flight speed for a particular animal from equation (10), provided that at least its weight and wing span are known. Substituting morphological relationships for wing characteristics given by Greenwalt (1962) for three bird groups : passerforms, shorebirds, and ducks into equation (10) a mass specific U_{mr} can be determined for each group. Although this division is based

Figure 15. Normalized relative to a solo flyer, equation 59 is plotted against different flock sizes, n . The benefit of flying in a flock of size $n = n_*$ is identical to that of flying solo: $R(1) = R(n_*)$. In this example, a member of a flock of size $n = n_{opt}$ is 60% more efficient than a solo flyer.



largely on disc loading, and not on taxonomy (Rayner, 1979), maximum range speed as a function to body mass for the three groups and all birds combined is given in table 1.

Substituting mass specific U_{mr} into equation (62) results in a mass specific optimum flock size. The corresponding flock size for the three groups and across all groups is given in column two of table 1. Since members in a group fall within a small range of mass, for example, the majority of ducks fall into a narrow range of about 1 kg, U_{mr} does not vary as greatly within a group as across a group. Accordingly, if birds within a group migrate similar distances then a small variation in flock size is to be expected. The interspecific equation for velocity (table 1) shows that a large variation in flock size is expected when comparing across a group then within a group. Although morphological relationships give a general trend, a more accurate measure of flock size can only be made when the values of T , U_{mr} and d are known for a specific species.

Flock size for various combinations of T , U_{mr} and d , are plotted in figure 16. Each panel, from left to right, is for a fixed T , 6, 12, and 18 hrs respectively, and is a plot of flock size vs distance, d (km), for three migration speeds. These panel show certain trends. First, for any fixed U_{mr} and d , flock size increases with increasing T . Second, for any given T and d , flock size increases with increasing U_{mr} . Finally, the critical distance at which to fly solo, irrespective of T , increases with higher cruising speed of the animal.

Seasonal Variation and Optimum Flock Size

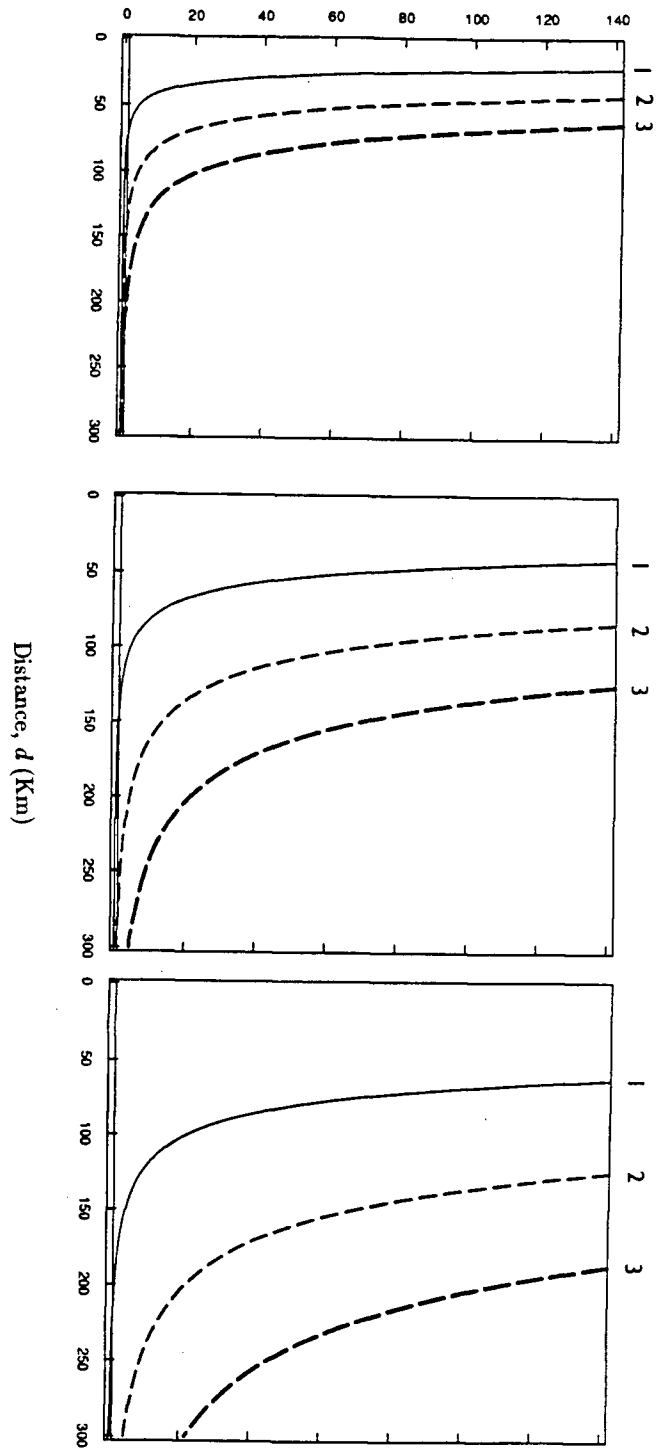
Total time available, T , is an important variable in determining optimum flock size. On any leg of the migration, T equals the sum of the airborne time, t_a and the foraging time, t_p . Day length, in some cases, may constrain the total time available to complete these two activities. Since day length changes with time of year, the optimum flock size at the time of the northward migration may differ from the size at the time of the return journey, on the southward migration. In other words, due

Table 1. Relation of maximum range speed to body mass, after Greenwalt (1962, 1975) and Rayner (1979). Optimum flock size is shown divided by $[T/d]^4$. (All quantities in MKS units.)

	Maximum range speed	Optimum flock size/ $[T/d]^4$
Interspecific rule	$10.04M^{0.24}$	$2.00 \times 10^3 M^{0.96}$
Intraspecific rule		
passiforms	$7.75 M^{0.11}$	$0.71 \times 10^3 M^{0.44}$
shorebirds	$8.98 M^{0.02}$	$1.28 \times 10^3 M^{0.08}$
ducks	$12.43M^{0.01}$	$4.71 \times 10^3 M^{0.04}$

Figure 16. Effect of T , d and U_{mr} on optimum flock size. Each panel, from left to right, is for a fixed T , 6, 12, and 18 hrs respectively, and is a plot of flock size vs distance, d (km) for $U_{mr} = 18$, 36 and 54 km/hr (1 – 3 respectively). Solid horizontal line corresponds to $n_{opt} = 1$, solo flight.

Optimum Flock Size (n_{opt})



to seasonal variation in day length there will be a corresponding change in flock size if T equals the number of hours between sunrise and sunset.

Hours of daylight depends on the solar declination and latitude of the observer (Griffiths, 1976). Solar declination, as a first approximation, is given by

$$\delta(t_j) = -23.5^\circ \cos \left(\frac{360 \cdot (t_j + 10)}{365.25} \right), \quad (72)$$

where t_j is the Julian date (Jan. 1 = 1, ... Dec. 31 = 365) in the year (Oke, 1987). Day length, hours between sunrise and sunset, is given by

$$H(\ell, t_j) = \frac{2}{15} \arccos(-\tan(\ell) \tan(\delta(t_j))), \quad (73)$$

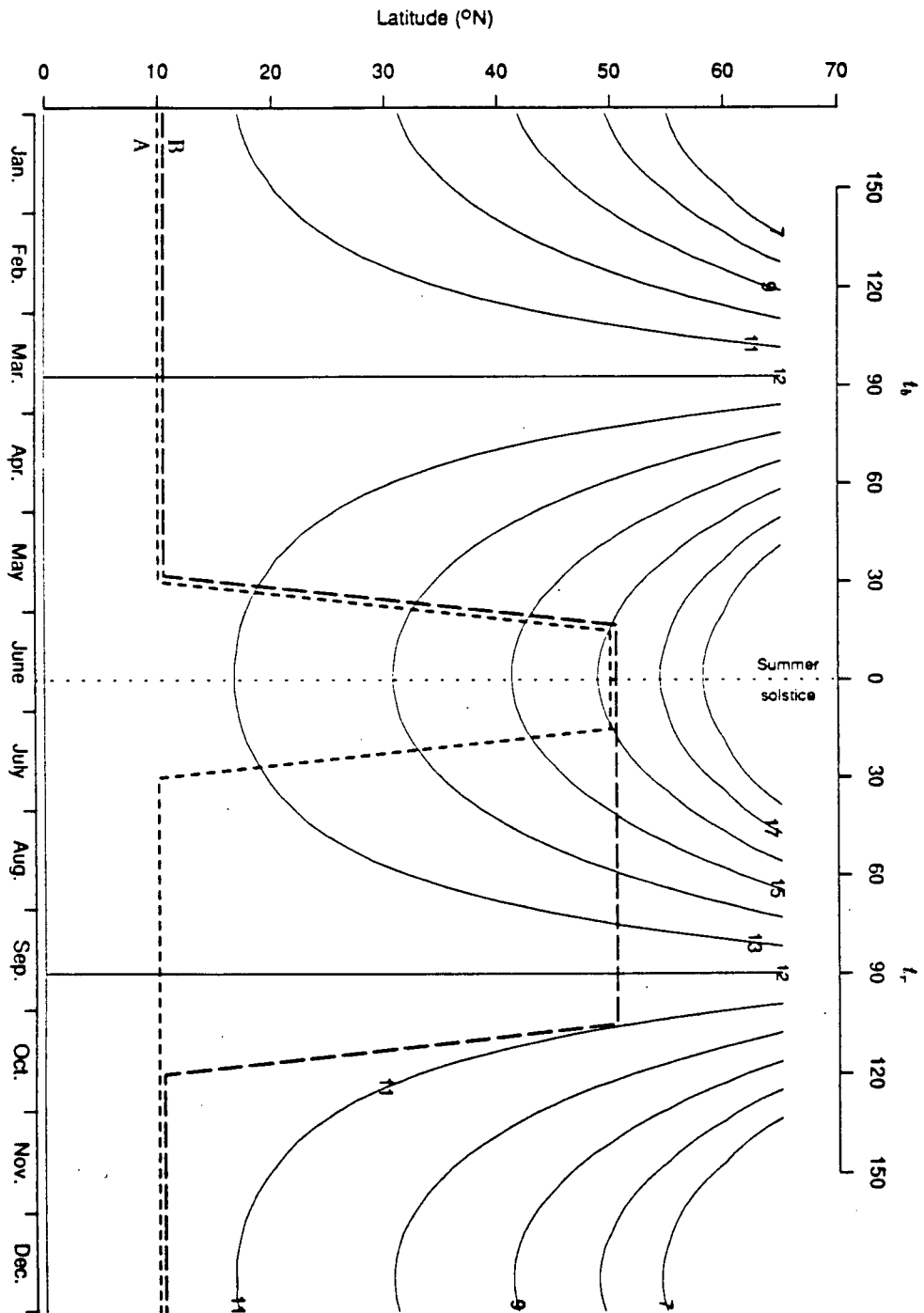
where ℓ is latitude, in degrees, and H is day length, in hours (Griffiths, 1976). Figure 17 illustrates the variation in day length with time of year and with latitude. From the beginning of the year, day length progressively gets longer, reaching 12-hours at the vernal equinox (March 21), and continually increases until the summer solstice (June 21), where it then starts to decrease, reaching again a 12-hour length at the autumn solstice (September 23). Over a year, this pattern of day length change is symmetrical about the summer solstice. In other words, days equidistant from the summer solstice have the same number of daylight hours, irrespective of latitude.

Now that T can be quantified by equation (73) it is interesting to study how it affects n_{opt} . Let the beginning of the northward migration be at time t_b , number of days before the summer solstice and let the return journey be at time t_r , number of days after the summer solstice. To a first approximation, and disregarding changes in hour length during the time of flight, the average number of hours of daylight from the start of the migration at latitude ℓ_1 at time t_j , to the end of the migration at latitude ℓ_2 can be calculated by

$$\bar{H}(t_j) = \frac{1}{\ell_2 - \ell_1} \int_{\ell_1}^{\ell_2} H(\ell, t_j) d\ell \quad (74)$$

(Greenspan and Benney, 1973). Substituting t_b and t_r for t_j in the above equation, gives the expected day length, $\bar{H}(t_b)$ and $\bar{H}(t_r)$, respectively, and can be assigned to

Figure 17. Contour of day length (hrs) with time of year and with latitude (solid lines). The dashed zigzag lines represent movement, from 10°N to 50°N, of two hypothetical migratory bird species. By flying equidistant number of days before and after the summer solstice (top axis), species A (short dash) will experience the same hour of day length on both the north and southward migration; consequently, no seasonal variation in flock size is to be expected. If the two phases occur in an asymmetrical pattern, as for species B (long dash), the average day length during the northward migration will be larger than the day length during the southward migration; as a result, seasonal variation in flock size is to be expected. The degree of variation in flock size is plotted in figure 18.



variable T in equation (62). Depending on the values of $\bar{H}(t_b)$ and $\bar{H}(t_r)$, optimum flock size for a given bird species may differ at time t_b from that at time t_r . Let R_s be the ratio of flock size at the the time of the northward migration to flock size at the time of the return journey. That is

$$R_s = \frac{\frac{16}{81} U_{mr}^4 \frac{\bar{H}(t_r)^4}{d^4}}{\frac{16}{81} U_{mr}^4 \frac{\bar{H}(t_b)^4}{d^4}} = \left[\frac{\bar{H}(t_r)}{\bar{H}(t_b)} \right]^4. \quad (75)$$

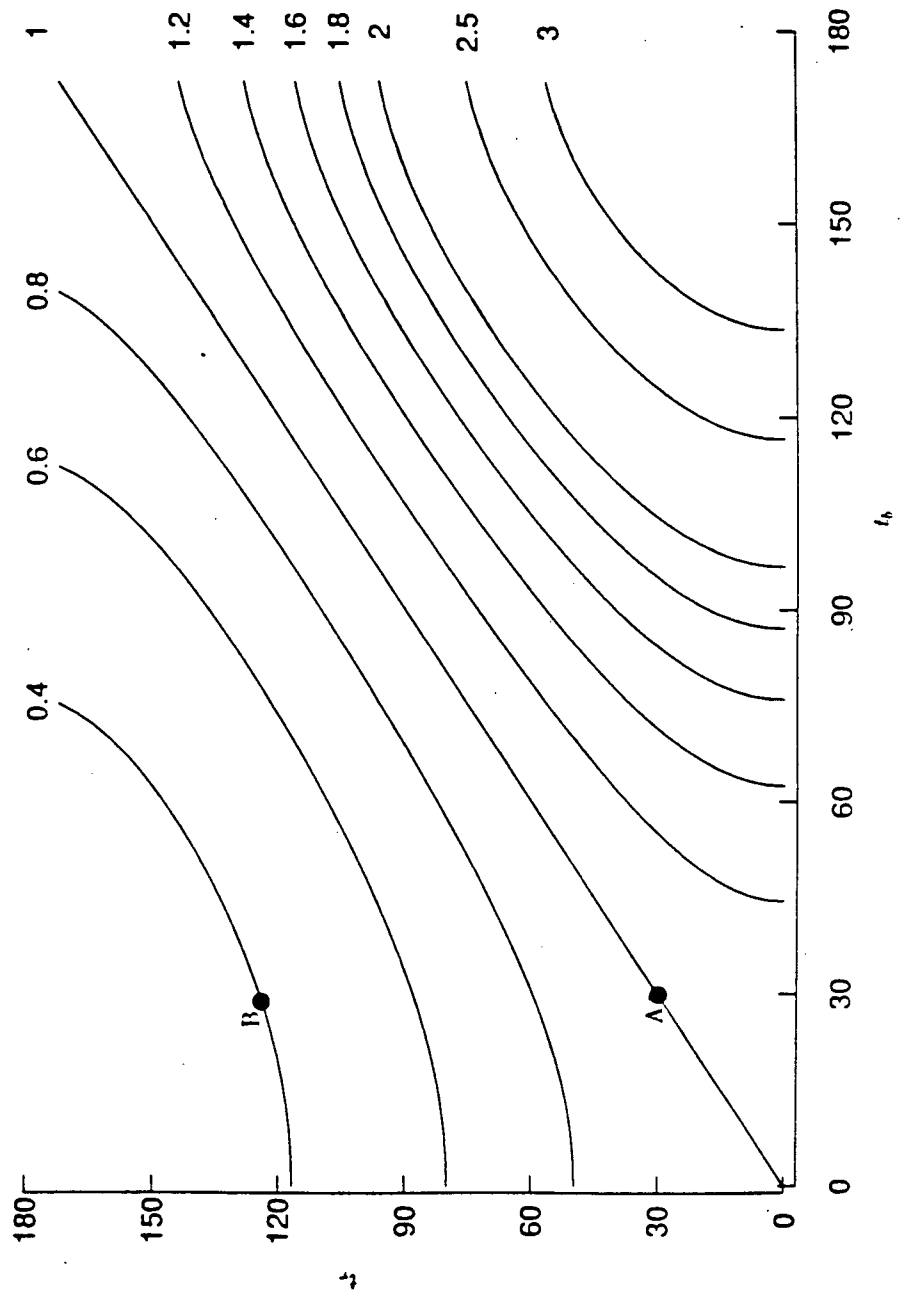
Using equation (74), the above equation can be written as

$$R_s = \left[\frac{\int_{\ell_1}^{\ell_2} H(\ell, t_r) d\ell}{\int_{\ell_1}^{\ell_2} H(\ell, t_b) d\ell} \right]^4. \quad (76)$$

The degree of seasonal variation in flock size can be implied from the above ratio. Contours of R_s are plotted against t_b and t_r in figure 18 for a bird species that migrates from $\ell_1 = 10^\circ\text{N}$ to $\ell_2 = 50^\circ\text{N}$. When the start and the return time is equidistant with respect to the summer solstice, there is no seasonal variation in flock size because the average number of day light hours is the same on both leg of the journey. In this case the ratio, R_s , equals one. Birds of similar migratory range, but of asymmetrical start and return time with respect of the summer solstice, however, should exhibit seasonal variation in flock size. The degree of this variation is expressed by the value of R_s . For example, if the start time is 30 days before and the return time is 120 days after the summer solstice then the flock size on the return journey from latitude 50°N to 10°N will be 40% smaller than that during the northward migration from 10°N to 50°N (point B, figure 18).

In conclusion, figure 18 shows that variation in flock size depends on the time of the north and southward migration with respect to the summer solstice. For bird species that migrate in a fashion where the north and southward migration times are symmetrical about the summer solstice no seasonal variation in flock size is expected. It is shown that asymmetrical time of the north and southward migration relative to the summer solstice is what causes variation in flock size. The degree of variation in flock size at these two times can be calculated from equation (76).

Figure 18. For migration from 10°N to 50°N , contours of the ratio R_s are plotted against t_b and t_r . The ratio R_s for bird species A and B is determined by the value of (t_b, t_r) pair which is (30,30) and (30,120) days respectively (see Figure 17). Ratio $R_s < 1$ corresponds to flock sizes being smaller during the southward migration compared to that during the northward migration. A ratio of one implies that flock sizes during the north and south migration are identical.



Discussion

Aerodynamic Model

The aerodynamic model of formation flight makes certain predictions on geometry, optimum speed and energy expenditure of a flock.

In terms of geometry, formation close to a crescent rather than a vee shape allows for equal distribution of induced drag reduction. In such a case, the crescent shape has approximately a formation angle (angle measured between the two legs of the formation) of 109° (Lassaman & Schollenberger, 1970). However, in most observed flocks the formation angle is much smaller than 109° , and the formation is in a distinct vee shape (Timothy et al. 1976; Gould & Heppner, 1974). This finding would imply that induced drag reduction is not equally distributed among members of a flock. Calculations by Hummel (1983) show that among all other birds in a formation the lead bird experiences the lowest induced drag reduction, while retaining a flying cost lower than a solo flyer. Taking turns leading during flight may be one way to assure that work is equally distributed within all members. No study as of yet has been done on the dynamics of birds within a flock although there are many accounts of birds changing lead position during flight.

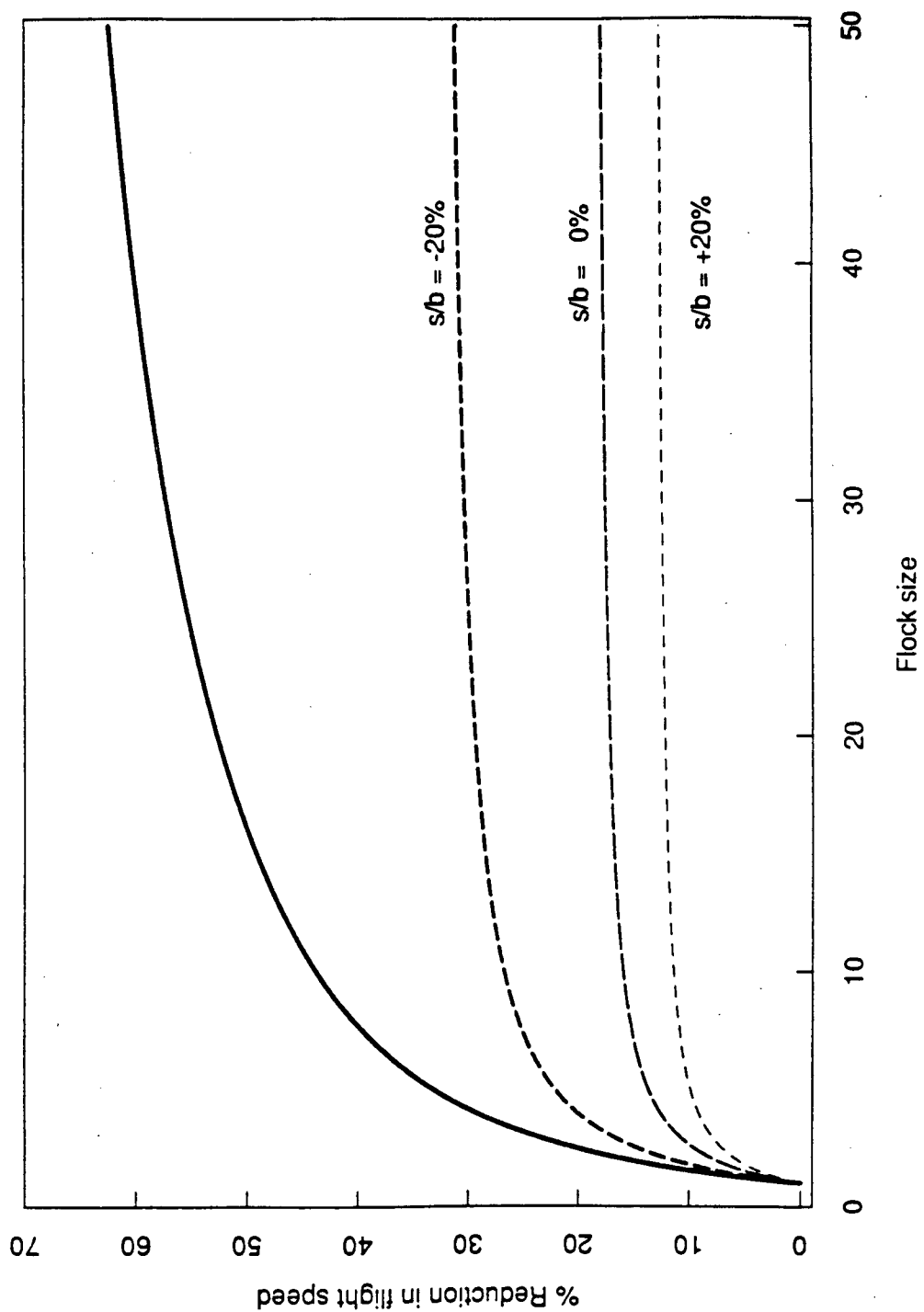
While distribution of induced drag reduction is influenced by formation angle the magnitude of this reduction is dependent on wing tip spacing (WTS). Within limits, tighter the formation higher the reduction in induced drag. By flying in a vee formation, certain overlap in WTS ($s < 0$) can occur which would be impossible, for example, in abreast formation. The limit of the overlap is determined by the position of the vortex filament shed from the bird ahead. A wing of semi-span b sheds two trailing vortex a distance $a = \frac{\pi}{4}b$ from the center of the wing (Houghton & Brock, 1970; Higdon & Corrsin, 1978). As shown in figure 7 the maximum induced drag reduction occurs when the trailing vortex of adjacent birds cancel each other out, corresponding to a WTS $s = 2(a - b)$. Observed WTS of Canada Geese (*Branta canadensis*) in two studies report a median WTS of -0.198 m (range -1.28

to 2.89 m) and -0.337 m (range -1.2 to 1.41 m) (Hainsworth, 1987; Hainsworth in press). Since in both studies it was assumed the birds were of constant length and of semi-wing span of $b = 0.75$ m, the corresponding predicted WTS is calculated to be $s = -0.36$ m. Although there is a large range of observed WTS, the latter study is in close agreement to the predicted WTS for maximum induced drag reduction. Large variation in observed WTS may be due to several factors such as local turbulence caused by change in wind direction or due to unpredictable moves by birds ahead (Hainsworth, 1988). While accounting for the dynamic nature of WTS between birds (see Figure 10, Hainsworth, 1988) the degree of overlap suggests that a relatively high reduction in induced drag can occur.

In order to achieve the best flight performance, all individuals of a flock must travel at an optimum speed. This speed, minimizing flying cost per unit distance flown, is a function of two variables, flock size, n and WTS, s . In general, optimum speed of a flock, $U_{mr}(n)$, is slower than that of a single bird, U_{mr} (Figure 19).

Specifically, equation 51 and C6 show that the optimum speed increases to the level of a single bird with increasing WTS or with decreasing flock size. In other words, the aerodynamic model predicts a negative correlation between speed and flock size for a given WTS. However, in three studies, two with Oystercatchers (*Haematopus ostralegus*) (Preuss, 1960; Noer, 1979) and one with Arctic Terns (*Sterna paradisaea*) (Alerstam, 1985), no significant correlation between speed and flock size was found. This apparent discrepancy between model and observation can be explained by the fact that all three studies failed to measure WTS, which affects optimum speed. For example, a 17% reduction in relative speed to a single bird is predicted for a flock containing 40 birds and 4 birds, at spacing $s/b = 0$ and $s/b = -20\%$ respectively. Not surprisingly then, no significant correlation can be established without knowledge of WTS. On the whole, any study to investigate the dependence of speed on flock size must measure WTS and other variables, such as wind speed and direction, which also effects optimum speed (Pennycuik, 1972).

Figure 19. Percent reduction in optimum flight speed relative to a single bird ($[U_{mr} - U_{mr}(n)]/U_{mr}$) at different flock size, n , and spacing index, s/b (s is WTS, b is semi-wing span). The solid line corresponds to a WTS when trailing vortices of adjacent bird cancel each other out.



Finally, the aerodynamic model predicts that formation flight be more advantageous than solitary flight in terms of energy expenditure. Observation on white pelicans (*Pelecanus erythrorhynchos*), commuting between nesting and foraging area, show lower flying cost for different types of formations if wingbeat is considered as an indicator of flying cost (O'Malley & Evans, 1982). The number of wingbeats per hour, calculated from wing beat frequency (beats per minute) and percent time flapping, was lowest in vee formation and greatest in single birds. It was found that birds in a vee formation had an average 6042 wingbeats/h whereas single birds flew with an average 7169 wingbeats/h (table 5; O'Malley & Evans, 1982) suggesting indirectly that formation flight provides aerodynamic advantage over solitary flight.

Optimum Flock Size Model

Verification of the model requires comparison with appropriate data. Four variables, WTS (s), cruising speed (U_{mr}), flight distance (d), and cumulative feeding and flying time (T) are interrelated components of this model. Presently, such data is sparse and where it exists it is often incomplete to validate this model. For example, many studies, while reporting flock size, are ambiguous about the behaviour of the flock. As is already known, there are many other types of behaviour that flocking is associated with, such as colonial nesting, communal roosting and anti-predator avoidance (McFarland, 1987), in addition to formation flight during migration. Clearly, a system to classify flock behaviour should be adapted to include behaviour of aerial flocks. For instance, formation flight is not restricted only to migration but may occur during local daily movements between nesting and foraging site, as in the case of Pelicans. Thus group flight may be associated with many types of behaviour. Here, model predicts size of migratory flock since non-migratory flock may travel at a speed different than maximum range speed (Pyke, 1981; Norberg 1981). Because literature information pertaining to this model is often incomplete, certain assumptions have to be made in order to determine optimum flock size of

migrating birds. Estimates of optimum flock sizes compared to what is observed in the field for cranes and Canada geese are considered next.

Although taking advantage of thermal soaring when meteorological conditions allow for it, common cranes' (*Grus grus*) primary mode of migration is powered flight, either in V or J flock formation (Pennycuick *et al.* 1979). In this species observed flock size range⁵ from 2 – 31 birds during part of spring migration from Rügen (54°30'N, 13°30'E), in the southern Baltic Sea, to lake Hornborgasjön (57°30'N, 14°02'E), in Sweden, a flight distance of nearly 400 km (Pennycuick *et al.* 1979). If flying and feeding is restricted between sunrise and sunset, the amount of time to complete these two activities during the April migration is approximately 13 hrs (Figure 17). Calculated maximum range speed for this species using a representative weight of 5.5 kg (Pennycuick *et al.* , 1979) is 55 km/hr (Table 1). Using field data to estimate flight distance ($d = 400$ km), general mathematical expressions to estimate both flight speed ($U_{mr} = 53$ km/hr) and day length ($T = 13$ hrs), and condition for maximum induced drag reduction to estimate WTS ($s = -0.43b$), gives an optimum number of 1.72 birds/flock (Equation (62)), a value near the lower range of observed size. Not all birds, however, make the journey in one day (Alerstam, 1974). Thus, if the journey is broken in two phases, with a single stopover 200 km away, the optimum number in this case ($d = 200$ km) is 27.6 birds/flock.

Likewise, using field data to estimate flight distance and speed allows calculations of optimum flock size in Whooping cranes (*Grus americana*) . By tracking daily movements of transmitter-tagged cranes along the Central flyway from Wood Buffalo National Park (58°30'N, 112°00'W), in Alberta to Aransas National Wildlife Refuge (26°30'N, 97°10'W), on the Texas Coast, the average distance between stopover sites was estimated to equal 325 km (Emanuel, 1982). From table 1, flight speed for this species was calculated at 58 km/hr, using an average male weight of 7.3 kg (Johnsgard, 1983). During fall migration period, between mid-October and early November, day length approximately equalled 10 hrs. Setting

$d = 325$ km, $U_{mr} = 58$ km/hr and $T = 10$ hrs in equation (62), gives an optimum number of 2 birds/flock. Central flyway fall migration records report flock size ranging from 1 – 9 birds, with an average of 2.6 birds/flock (Table 2, Johnsgard, 1983).

Finally, migration timing and distance data on a population of Canada Geese (*Branta canadensis*), which nests at Marshy Point Goose Sanctuary (50°32'N, 98°07'W), Manitoba and migrate to Silver Lake (44°00'N, 92°20'W) in Rochester, Minnesota (Wege & Raveling, 1983), allow the estimation of seasonal variation in flock size and the determination of conditions for solo and group flight. The data shows that transmitter-tagged geese took on an average 8.3 and 2.3 days during the spring (8 – 15 April) and autumn (28 Oct. – 2 Nov.) migrations respectively to complete the 855 km journey between Lake Rochester and Marshy Point Goose Sanctuary. On the average birds flew 371 km, with some flying non-stop during the autumn migration period. In contrast, all the tagged geese interrupted their spring migration. In fact because stopover areas in the spring were pastures and gain fields, many birds broke the migration to renew fat reserves while advancing northward (Elkins, 1988; Wege & Raveling, 1983). As a result, map locations of stopover sites were used to estimate flight distance (Fig. 2, Wege & Raveling, 1983). On the average birds flew 170 km during the spring migration period, about 50% less than on their southward migration. Hours of daylight also differed during the two migration periods and was equal to 14 and 11 hrs at the time of the north and southward migrations respectively. Figure 20 shows predicted flock size during the spring and autumn migration for varying distance between stopover sites. For this case, the figure shows two trends: firstly, that there is a seasonal variation in flock size, with flocks being largest in the spring and secondly, that flock size should decrease as the distance between stopover sites increase, with the possibility of flying solo. Data on flock size, while lacking in Wege & Raveling (1983) study, is varied. For example, data collected in central Illinois report flock size ranging from 23 – 300 birds, with an average of 96 birds/flock (Bellrose, 1980). Other studies

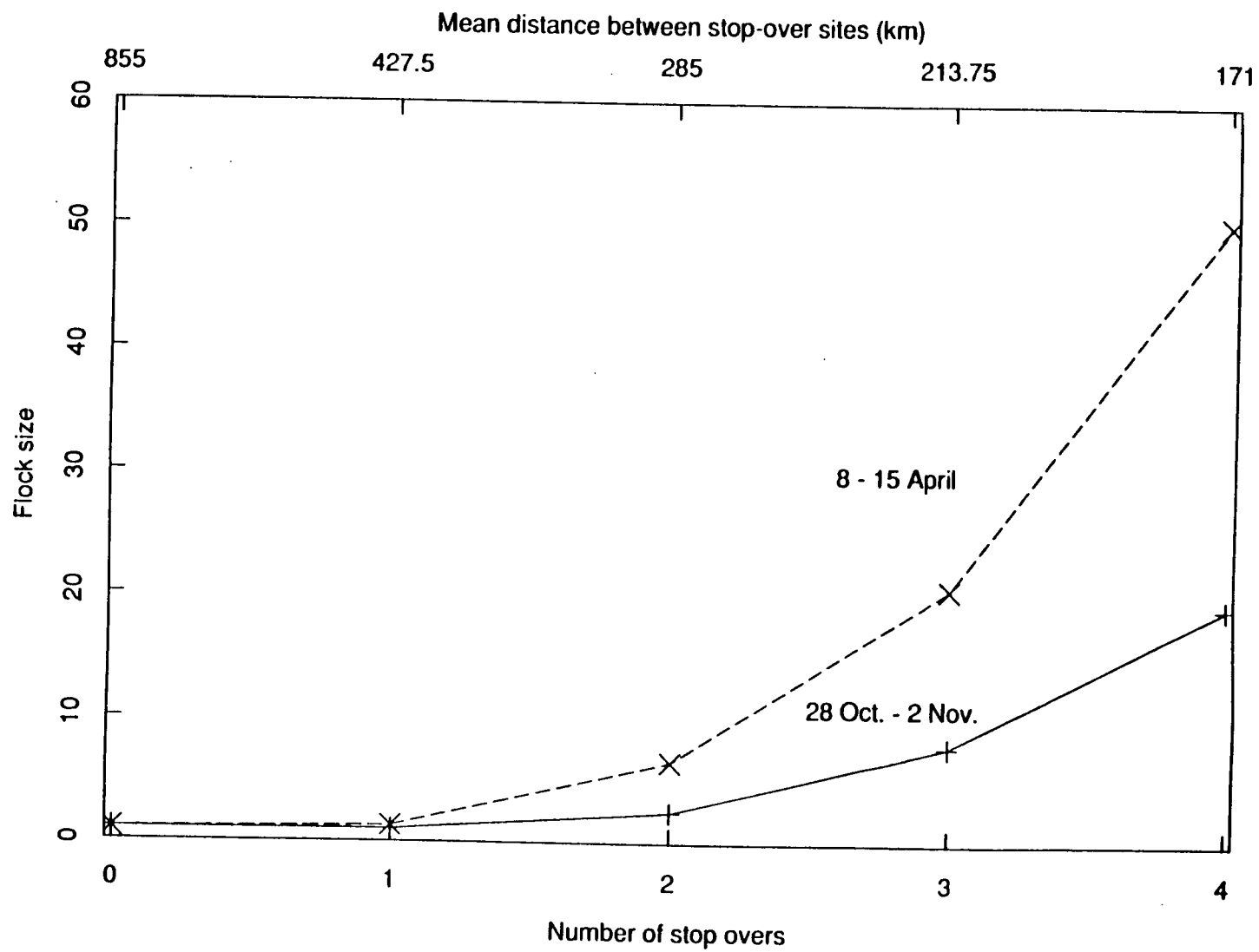
report for this species an average size of 36.08 (Wing, 1941), 27.02 (Heppner, 1974) and 5 birds/flock (Elder & Elder, 1949). On the whole, it is predicted that Canada Geese may migrate in flocks that are highly variable in size, determined, among other factors, by distance between stopover sites and time of year.

It is recognized that a number of assumptions have been made in determining optimum flock size. Nevertheless, the estimates of flock size agree with what is observed in the field, and supply an understanding, if tentative, basis for interpreting flock size in migrating birds.

Not all birds migrate in flocks. Condition for solo flight admittedly depends on the value of U_{mr} , T and d . However, since flock size approaches a value equal to one with increasing flight distance, this distance largely determines solo flight condition for the case of long non-stop migration. In such cases flight distance can be thousands of kilometres, often over uninhabitable regions such as oceans, deserts, and glaciers and flight time may range from 20 to 100 hours, depending on the energy reserve of the migrant (Alerstam, 1976). To illustrate, geese travel long distances non-stop, such as the lesser snow geese (*Anser caerulescens*) in North America which fly from James Bay to the Gulf of Mexico, a distance of about 2700 km in 60 h and the Brant geese (*Branta bernicla*) which fly about 4000 km across the Pacific Ocean from the Alaska Peninsula to South California coast (Ogilvie, 1978). Other bird species such as the European cuckoo fly over 3000 km from southern Europe to equatorial Africa migrate singly or in small flocks (Wyllie, 1981). Likewise, travelling singly or in a small group, Pacific Golden Plover fly approximately 4000 km over open ocean from Alaska to Hawaii (Johnston & McFarlane, 1967). On the whole, for the case of long non-stop migration, the model predicts solo flight as a possible migration strategy.

The approach taken here allows the determination of aerial flock sizes in migrating birds. However, the model can accommodate more detailed information on a variety of issues. Specifically, observation of flocks sizes for different bird species,

Figure 20. Predicted optimum flock size during the spring and autumn migration for varying distances between stop-over sites (top axis) or equivalently the number of stop-overs required to complete the 855 km journey (bottom axis). See text for detail.



and under different migration conditions would be rewarding. Further detailed work on seasonal time budget of migrating birds and their flight speed is still needed. Eventually, this would provide a basis of for comparative study of flock sizes for different migrating species and for different times of the year. In addition, several aspects of the aerodynamic model such as the optimal adjustment of air speed for different flock size and WTS still needs to be explored.

Summary

- (i) The aerodynamic of formation flight theory for a fixed wing aircraft has been applied to avian formation flight. Two approximation techniques are derived which greatly simplify induced drag calculations for a single bird flying in a group of n birds at wing-tip spacing s . The approximation formula guarantees the relative error to be less than 23% for spacing index greater than $s/b = -20\%$. Relative error decreases with increasing n and s .
- (ii) The results show that a striking saving in induced drag can occur during formation flight. Typically, a group of 25 birds in tip-to-tip formation (i.e. $s = 0$) has approximately 50% reduction in induced drag than a lone bird. The greatest reduction in induced drag occurs in formations where tip vortices of adjacent birds overlap. In such formations, induced drag for a member of a flock is $1/n$ th the induced drag of a single bird.
- (iii) Maximum range speed of a flock decreases with flock size. For a group of 25 birds in tip-to-tip formation there is approximately a 15% reduction in optimal speed relative to a single bird. In formations where tip vortices of adjacent birds overlap, maximum range speed of a flock is reduced by a factor of $(1/n)^{1/4}$.
- (iv) The optimum flock size model is based on the energetic cost of flight and energy income from foraging. Optimum size of a flock is a function of four variables: s , U_{mr} , T and d .
- (v) If migration is constrained by hours of daylight, no seasonal variation in flock size is expected if north and southward migration times are symmetrical with respect to the summer solstice. If, however, these two timings are asymmetrical, then the variation in flock size is dependent on the ratio of day length during the northward migration to that of the southward migration.
- (vi) Under certain conditions, such as long non-stop migration, solo flight is an optimum migratory strategy.

References

- ALERSTAM, T. (1976) The course and timing of bird migration. Pp. 9 – 54 in D.J. Aidley (ed.) *Animal migration*. Cambridge Univ. Press.: Cambridge.
- ALERSTAM, T. (1985) Strategies of migratory flight, illustrated by arctic and common terns, *Sterna paradisaea* and *Sterna hirundo*. Pp. 580 – 617 in M.A. Rankin (ed.) *Migration: Mechanism and adaptive significance*. Marine Science, Institute, Texas.
- BADGEROW, J.P. AND F.R. HAINSWORTH (1984) Energy savings from formation flight. A re-examination of the vee formation *J. Theor. Biol.* **93**: 41 – 52.
- BELLROSE, F.C. (1980) *Ducks, geese & swans of North America*. Stackpoole Books: Harrisburg, Pa.
- BILL, R.G. AND W.F. HERNNKIND (1976) Drag reduction by formation movement in spiny lobsters. *Science* **193**: 1146 – 1148.
- BYKHOVSKII, B.E. (1973) *Bird migrations*. John Wiley & Sons: New York.
- CLOUDSLEY-THOMPSON, J. (1978) *Animal migration*. Orbis Publishing: London.
- DORST, J. (1962) *The migration of birds*. Houghton Mifflin Company: Boston.
- ELKINS, N. (1988) *Weather and bird behaviour*. T & A D Poyser: Calton, England.

Optimum Bird Flock Size in Formation Flight

- DUNNING, J.B. (1984) Body weight of 686 species of North American birds. Western Bird Banding Association. Monograph No. 1, May 1984.
- ELDER, W.H. AND N.L. ELDER (1949) Role of the family in the formation of goose flocks. *Wilson Bulletin* **61**: 133 – 140.
- ELLINGTON, C.P. (1984) The aerodynamics of hovering insect flight. *Phil. Trans. Royal. Soc. Lond.* **305(1122)**: 1 – 181.
- EMANUEL, V.L. (1982) South Texas region. *American Birds* **36(2)**: 194 – 197.
- FRANZISKET, L. (1951) Über die ursachen formationsfluges. *Vogelwarte* **16**: 48 – 55.
- GOULD, L.L. AND F. HEPPNER (1974) The Vee formation of Canada geese. *Auk* **91**: 494 – 505.
- GREENSPAN, H.P. AND D.J. BENNEY (1973) *Calculus an introduction to applied mathematics*. McGraw-Hill: New York.
- GREENEWALT, C.H. (1962) Dimensional relationships for flying animals. *Smith. Misc. Coll.* **144(2)**: 1 – 45.
- GREENEWALT, C.H. (1975) The flight of birds. The significant dimensions, their departure from the requirement for dimensional similarity, and the effect on flight aerodynamics of that departure. *Trans. Amer. Phil. Soc.* **65(4)**: 1 – 67.
- GRIFFIN, D.R. (1964) *Bird migration*. Anchor Books: New York.

- GRIFFITHS, J.F. (1976) *Climate and the environment: the atmosphere impact on man*. P. Elek: London.
- HAMILTON, W.J. III (1967) Social aspects of bird orientation mechanism. Pp. 57 – 69 in R.M. Storm (ed.) *Animal orientation and navigation*. Oregon State Universtiy Press: Corvallis, OR.
- HAINSWORTH, F.R. (1990) Wing movements and postioning for aerodynamic benefit by Canada geese flying in formation. (in press).
- HAINSWORTH, F.R. (1988) Induced drag savings from ground effect and formation flight in brown pelicans. *J. exp. Biol.* **135**: 431 – 444.
- HAINSWORTH, F.R. (1987) Precision and dynamics of positioning by Canada geese flying in formation. *J. Exp. Biol.* **128**: 445 – 462.
- HIGDON, J.J.L. AND S. CORRSIN (1978) Induced drag of a bird flock. *Am. Nat.* **112**: 727 – 744.
- HOUGHTON, E.L. AND A.E. BROCK (1960) *Aerodynamics for engineering students*. Edward Arnold: London.
- HUMMEL, D. (1983) Aerodynamic aspects of formation flight in birds. *J. Theor. Biol.* **104**: 321 – 347.
- HUMMEL, D. AND M. BEUKENBERG (1989) Aerodynamische interferenzefekte beim formationsflug von vögelin. *I. Orn.* **130**: 15 – 24.
- HYSLOP, J.M. (1954) *Infnite series*. Oliver and Boyd: London.

- JOHNSGARD, P.A. (1983) *Cranes of the world*. Indiana University Press: Bloomington.
- JOHSTON, D.W. AND W. MCFARLANE (1967) Migration and bioenergetics of flight in the pacific golden plover. *The Condor* **69**: 156 – 168.
- KEETON, W.T. (1970) Comparative observations and homing performance of single pigeons and small flocks. *Auk* **87**: 797 – 799.
- KOKSHAYSKY, N.V. (1979) Tracing the wake of a flying bird. *Nature* **279**: 146 – 148.
- LISSAMAN, P.B.S. AND C.A. SCHOLLENBERGER (1970) Formation flight of birds. *Science* **168**: 1003 – 1005.
- LUGT, H.I. (1983) *Vortex flow in nature and technology*. John Wiley & Sons: New York.
- MILNE-THOMSON, L.M. (1973) *Theoretical aerodynamics*. Dover Publications: New York.
- MANGEL, M AND W.C. CLARK (1988) *Dynamic modelling in behavioral ecology*. Princeton University Press: Princeton.
- MCCORMICK, B.W. (1979) *Aerodynamics, aeronautics, and flight mechanics*. John Wiley & Sons: New York.
- MCFARLAND D. (1987) *Animal Behaviour*. Oxford University Press: Oxford.
- MEAD, C. (1983) *Bird migration*. Newnes Books: Great Britain.

- MORAN, J. (1984) *An introduction to theoretical and computational aerodynamics*. John Wiley & Sons: New York.
- NOER, H. (1979) Speeds of migrating waders *Charadriidae*. *Dansk orn. Foren. Tidsskr.* **73**: 215 – 224.
- NORBERG, R.A. (1981) Optimal flight speed in birds when feeding young. *J. Animal. Ecol.* **50**: 473 – 477.
- O'MALLEY, J.B.E. AND R.M. EVANS (1982) Structure and behavior of white pelican formation flocks. *Can. J. Zool.* **60**: 1388 – 1396.
- OKE, T.R. (1987) *Boundary layer climates*. Methuen: London.
- PENNYCUICK, C.J. (1969) The mechanics of bird migration. *Ibis* **111**: 525 – 556.
- PENNYCUICK, C.J. (1972) *Animal Flight*. Edward Arnold: London.
- PENNYCUICK, C.J. (1978) Fifteen testable predictions about bird flight. *Oikos* **30**: 165 – 176.
- PENNYCUICK, C.J., T. ALERSTAM AND B. LARRSON (1979) Soaring migration of the common crane *Grus grus* observed by radar and from an aircraft. *Ornis scandinavica* **10**: 241 – 251.
- PRANDTL, L. AND O.G. TIETJENS (1957) *Fundamentals of hydro and aeromechanics*. Dover Publications: New York.

- PREUSS, N.O. (1960) Ground-speed and air-speed according to flock size in migrating birds. *Dansk. orn. Foren. Tidsskr.* **54**: 136 – 143.
- PYKE, G.H. (1981) Optimal travel speeds of animals. *Am. Nat.* **118**: 475 – 487.
- PYKE, G.H., PULLIAM H.R. AND E.L. CHARNOV (1977) Optimal foraging: a selective review of theory and tests. *Q. Rev. Biol.* **52**: 137 – 154.
- RANKIN, M.A. (1985) *Migration: mechanisms and adaptive significance*. Marine Science Institute: Austin.
- RAYNER, J.M.V. (1979a) A new approach to animal flight mechanics. *J. Exp. Biol.* **80**: 17 – 54.
- RAYNER, J.M.V. (1979b) A vortex theory of animal flight. I. The vortex wake of a hovering animal. II. The forward flight of birds. *J. Fluid Mech.* **91**: 697 – 730; 731 – 763.
- RAYNER, J.M.V. AND J.N. ALDRIDGE (1985) Three-dimensional reconstruction of animal flight paths and turning flight of microchiropteran bats. *J. Exp. Biol.* **118**: 247 – 265.
- RAYNER, J., JONES, G., AND A. THOMAS (1986) Vortex flow visualizations reveal change in upstroke function with flight speed in bats. *Nature* **321**: 162 – 164.
- REID, E.G. (1932) *Applied wing theory*. McGraw – Hill: New York.

- SCHLICHTING, H. AND E. TRUCKENBRODT (1979) *Aerodynamics of the airplane*. McGraw Hill: New York.
- SCHMID – HEMPEL, P., KACELNIK, A. AND HOUSTON (1985) Honeybees maximize efficiency by not filling their crop. *Behav. Ecol. Sociobiol* **17**: 61 – 66.
- SCHMIDT – KOENIG, K. (1979) *Avian Orientation and navigation*. Academic Press: London.
- SCHOENER, T.W. (1971) Theory of feeding strategies. *Ann. Rev. Ecol. Syst.* **11**: 369 – 404.
- SIBLEY, R.M. (1983) Optimal group size is unstable. *Animal Behaviour* **31**: 947 – 948.
- SPEDDING, G.R., RAYNER, J.M.V., AND C.J. PENNYCUICK (1984) Momentum and energy in the wake of a pigeon (*Columba livia*) in slow flight. *J. Exp. Biol.* **111**: 81 – 102.
- SPEDDING, G.R. (1987) The wake of a kestrel (*Falco tinnunculus*) in flapping flight. *J. Exp. Biol.* **127**: 59 – 78.
- TAYLOR, J (1982) *An introduction to error analysis*. University Science Books: Mill Valley, California.
- TALAY, T. (1975) *Introduction to the aerodynamics of flight*. National Aeronautics and Space Administration: Washington, D.C.

- TOKATY, G.A. (1971) *A history and philosophy of fluidmechanics*. G.T. Foulis & Co. Ltd.: Oxfordshire.
- TUCKER, V.A. (1973) Bird metabolism during flight: Evaluation of a theory. *J. Exp. Biol.* **58**: 689 – 709.
- VINE, I. (1971) Risk of visual detection and pursuit by predator and the selective advantage of flocking behaviour. *J. theor. Biol.* **30**: 405 – 422.
- WARD-SMITH, A.J. (1984) *Biophysical aerodynamics and the natural environment*. John Wiley & Sons: New York.
- WEGE, M.L. AND D.G. RAVELING (1983) Factors influencing the time, distance, and path of migrations of Canada geese. *Wilson Bull.* **95**(2): 209 – 221.
- WEIHS, D. (1973) Hydromechanics of fish schooling. *Nature* **241**: 290 – 291.
- WETMORE, A. (1930) *The migrations of birds*. Harvard University Press: Cambridge.
- WIESELSBERGER, C. (1914) Z. Flugtech. *Motorluftschiff* **5**: 225 – 227.
- WILLIAMS T., KLONOWSKI T. AND P. BERKELY (1976) Angle of Canada goose V flight formation measured by radar. *Auk* **93**: 554 – 559.
- WING L. (1941) Size of bird flocks in winter. *Auk* **58**: 188 – 194.
- WYLLIE, I. (1981) *The cuckoo*. Universe Books: New York.

Appendix A

Limiting Case as $n \rightarrow \infty$

Induced drag of a bird in a flock of size n is

$$\bar{D}_I(n) = D_I + \frac{2}{n} \sum_{i=1}^{n-1} \sum_{j=i+1}^n D_{Iij} \quad (A1)$$

Substituting equation (34) for D_{Iij} , the second term of the above equation can be written as

$$\sum_{i=1}^{n-1} \sum_{j=i+1}^n D_{Iij} = \frac{2D_I}{\pi^2} \sum_{i=1}^{n-1} \sum_{j=i+1}^n \log \left[1 - \left(\frac{2a}{|i-j|(2b+s)} \right)^2 \right] \quad (A2)$$

Applying the logarithm law,

$$\begin{aligned} \log(u_1) + \log(u_2) + \dots + \log(u_n) &= \log(u_1 u_2 \dots u_n) \\ \sum_{i=1}^n \log[u_i] &= \log \left[\prod_{i=1}^n u_i \right] \end{aligned} \quad (A3)$$

to the inner summation, gives

$$\sum_{i=1}^{n-1} \sum_{j=i+1}^n D_{Iij} = \frac{2D_I}{\pi^2} \sum_{i=1}^{n-1} \log \left[\prod_{j=i+1}^n \left[1 - \left(\frac{2a}{|i-j|(2b+s)} \right)^2 \right] \right] \quad (A4)$$

Let $k = |i-j|$ then

$$= \frac{2D_I}{\pi^2} \sum_{i=1}^{n-1} \log \left[\prod_{k=1}^n \left[1 - \left(\frac{2a}{k(2b+s)} \right)^2 \right] \right] \quad (A5)$$

As $n \rightarrow \infty$, the upper limit of product term changes from n to ∞ , that is

$$= \frac{2D_I}{\pi^2} \sum_{i=1}^{n-1} \log \left[\prod_{k=1}^{\infty} \left[1 - \left(\frac{2a}{k(2b+s)} \right)^2 \right] \right] \quad (A6)$$

Given the identity,

$$\frac{\sin(x)}{x} = \prod_{k=1}^{\infty} \left[1 - \left(\frac{x}{\pi k} \right)^2 \right] \quad (A7)$$

(Hyslop, 1954) the infinite product term can be written as

$$\prod_{k=1}^{\infty} \left[1 - \left(\frac{x}{\pi k} \right)^2 \right] = \frac{\sin(2a\pi/(2b+s))}{2a\pi/(2b+s)} \quad (A8)$$

where, in this case,

$$x = \frac{2a\pi}{2b+s} \quad (A9)$$

Now, the double summation can be expressed as

$$\sum_{i=1}^{n-1} \sum_{j=i+1}^n D_{Iij} = \frac{2D_I}{\pi^2} \sum_{i=1}^{n-1} \log \left[\frac{\sin(2a\pi/(2b+s))}{2a\pi/(2b+s)} \right] \quad (A10)$$

Since the terms in the summation on the r.h.s. are independent of the index i , the preceding equation can be written as

$$\sum_{i=1}^{n-1} \sum_{j=i+1}^n D_{Iij} = \frac{2D_I}{\pi^2} (n-1) \log \left[\frac{\sin(2a\pi/(2b+s))}{2a\pi/(2b+s)} \right] \quad (A11)$$

Substituting the double summation of equation A1 with the above result gives

$$\bar{D}_I(n) = D_I + \frac{4D_I}{\pi^2} \frac{(n-1)}{n} \log \left[\frac{\sin(2a\pi/(2b+s))}{2a\pi/(2b+s)} \right] \quad (A12)$$

Consequently, as $n \rightarrow \infty$, $(n-1)/n \rightarrow 1$. Thus

$$\lim_{n \rightarrow \infty} \bar{D}_I(n) = D_I + \frac{4D_I}{\pi^2} \log \left[\frac{\sin(2a\pi/(2b+s))}{2a\pi/(2b+s)} \right] \quad (A13)$$

Appendix B

Approximation Technique

The goal of the approximation technique is to represent the total induced drag of a flock of size n (equation B1) in a close form; in other words, by an analytic function. Figure 9 gives a pictorial representation of the approximation technique.

Specifically, in a formation of n birds, the left and right most birds are assumed to be flanked on either the starboard or port, respectively, by an infinite number of birds. The remaining birds, having neighbors on both sides, are assumed to be

flanked on both the port and starboard by infinite number of birds. Following the above assumptions, the total induced drag,

$$D(n) = nD_I + 2 \sum_{i=1}^{n-1} \sum_{j=i+1}^n D_{Iij}, \quad (B1)$$

can be decomposed into

$$D(n) \approx nD_I + 2 \sum_{j=2}^{\infty} D_{I1j} + 2 \sum_{i=2}^{n-1} \sum_{j=i+1}^{\infty} D_{Iij} \quad (B2)$$

Calculation of the first and second summation series gives the total mutual induced drag for the two end birds, and for the remaining $n - 2$ birds within the flock, respectively.

Substituting equation (34), for D_{I1j} the first summation series can be written as

$$\sum_{j=2}^{\infty} D_{I1j} = \frac{2D_I}{\pi^2} \sum_{j=2}^{\infty} \log \left[1 - \left(\frac{2a}{|1-j|(2b+s)} \right)^2 \right] \quad (B3)$$

with some manipulation (see Appendix A) it can be expressed as

$$\sum_{j=2}^{\infty} D_{I1j} = \frac{2D_I}{\pi^2} \log \left[\prod_{k=1}^{\infty} \left[1 - \left(\frac{2a}{k(2b+s)} \right)^2 \right] \right] \quad (B4)$$

Using the identity in Appendix A, the above equation reduces to

$$\sum_{j=2}^{\infty} D_{I1j} = \frac{2D_I}{\pi^2} \log \left[\frac{\sin(2a\pi/(2b+s))}{2a\pi/(2b+s)} \right] \quad (B5)$$

In a similar fashion, the second summation series

$$\sum_{i=2}^{n-1} \sum_{j=i+1}^{\infty} D_{Iij} = \frac{2D_I}{\pi^2} \sum_{i=1}^{n-1} \log \left[\prod_{k=1}^{\infty} \left[1 - \left(\frac{2a}{k(2b+s)} \right)^2 \right] \right] \quad (B6)$$

can be reduce to (see Appendix A)

$$\sum_{i=2}^{n-1} \sum_{j=i+1}^{\infty} D_{Iij} = \frac{2D_I}{\pi^2} \sum_{i=2}^{n-1} \log \left[\frac{\sin(2a\pi/(2b+s))}{2a\pi/(2b+s)} \right] \quad (B7)$$

Since each term in the above summation is independent of the index i , the above equation simplifies to

$$\sum_{i=2}^{n-1} \sum_{j=i+1}^{\infty} D_{Iij} = \frac{2D_I}{\pi^2} (n-2) \log \left[\frac{\sin(2a\pi/(2b+s))}{2a\pi/(2b+s)} \right] \quad (B8)$$

Substituting the first and second summation series of equation B2 by the above results (equations B5 and B8 respectively) gives

$$D_I(n) \approx nD_I + \frac{4D_I}{\pi^2} \log \left[\frac{\sin(2a\pi/(2b+s))}{2a\pi/(2b+s)} \right] + \frac{4D_I}{\pi^2} (n-2) \log \left[\frac{\sin(2a\pi/(2b+s))}{2a\pi/(2b+s)} \right] \quad (B9)$$

Grouping terms, gives an approximation function to the total induced drag of a flock of size n (equation B1)

$$D_I(n) \approx nD_I + \frac{4D_I}{\pi^2} (n-1) \log \left[\frac{\sin(2a\pi/(2b+s))}{2a\pi/(2b+s)} \right] \quad (B10)$$

Accordingly, the average induced drag, $\bar{D}_I = D_I(n)/n$, is

$$\bar{D}_I(n) \approx D_I + \frac{4D_I}{\pi^2} \frac{(n-1)}{n} \log \left[\frac{\sin(2a\pi/(2b+s))}{2a\pi/(2b+s)} \right] \quad (B11)$$

Appendix C

Optimum Flock Size as a Function of Wing-tip Spacing

Energy expenditure for a bird in formation flight is given by

$$E_{out} = (D_P + \bar{D}_I(n))d, \quad (C1)$$

where in this case

$$\bar{D}_I(n) = D_I(A + B/n) \quad (C2)$$

and

$$A = 1 + \frac{4}{\pi^2} \log \left[\frac{\sin(\beta)}{\beta} \right], \quad (C3)$$

$$B = -\frac{4}{\pi^2} \log \left[\frac{\sin(\beta)}{\beta} \right], \quad (C4)$$

with $\beta = 2a\pi/(2b + s)$. Thus

$$E_{out} = (D_P + D_I(A + B/n))d. \quad (C4)$$

Substituting equation (2) and (3) for D_P and D_I respectively, and grouping terms gives

$$E_{out} = (k_p U^2 + k_i(A + B/n)U^{-2})d. \quad (C5)$$

The optimum cruising speed is given by

$$U_{mr}(n) = \left(\frac{k_i}{k_p}\right)^{1/4} (A + B/n)^{1/4}. \quad (C6)$$

Airborne time to fly a distance d is

$$t_a = d \left(\frac{k_i}{k_p}\right)^{1/4} \left(\frac{n}{An + B}\right)^{1/4}. \quad (C7)$$

Finally, the flying cost at $U = U_{mr}(n)$ is

$$E_{out} = 2d\sqrt{k_i k_p} \sqrt{A + B/n}. \quad (C8)$$

E_{in} is given by

$$E_{in} = \lambda(T - t_a). \quad (C9)$$

Substituting equation C7 for t_a in the above equation gives

$$E_{in} = \lambda \left(T - d \left(\frac{k_p}{k_i}\right)^{1/4} (A + B/n)^{1/4} \right) \quad (C10)$$

The ratio

$$R(n) = \frac{E_{in}}{E_{out}} = \frac{\lambda \left(T - d \left(\frac{k_p}{k_i}\right)^{1/4} (A + B/n)^{1/4} \right)}{2d\sqrt{k_i k_p} \sqrt{A + B/n}}. \quad (C11)$$

Differentiating the above ratio with respect to n gives

$$\frac{dR(n)}{dn} = \frac{B\lambda \left(2k_i^{1/4} n^{3/4} (An + B)^{1/4} T - 3dk_p^{1/4} n \right)}{8dk_i^{3/4} k_p^{1/2} n^{5/4} (An + B)^{7/4}} = 0. \quad (C12)$$

Finally, solving for n gives the optimum flock size as a function of wing-tip spacing,

$$n_{opt}(s) = \frac{B}{\frac{81}{16} \frac{k_p}{k_i} \left(\frac{d}{T}\right)^4 - A} \quad (C13)$$

since both A and B are a function of s (Equations C3 & C4). Finally, substituting equation (62) in the above equation gives

$$n_{opt}(s) = \frac{B}{1/n_{opt} - A}$$

Appendix D

Upper Bound for Maximum Flock Size

Let the maximum flock size n_* be the flock size at which a member of a flock has the same benefit as a solo flyer. That is

$$\frac{\lambda \left(T - d \left[\frac{k_p}{k_i} \right]^{1/4} \right)}{2d \sqrt{k_p \cdot k_i}} = \frac{\lambda \sqrt{n_*} \left(T - d \left[\frac{k_p}{k_i} \right]^{1/4} n_*^{1/4} \right)}{2d \sqrt{k_p \cdot k_i}}. \quad (D1)$$

Solving for n_* ,

$$\sqrt{n_*} = 1 + \frac{d}{T} \cdot \left[\frac{k_p}{k_i} \right]^{1/4} n_*^{3/4} - \frac{d}{T} \cdot \left[\frac{k_p}{k_i} \right]^{1/4}. \quad (D2)$$

Given that $U_{mr} = (k_i/k_p)^{1/4}$ the above equation can be written as

$$\sqrt{n_*} = 1 + \frac{d}{T} \cdot \frac{n_*^{3/4}}{U_{mr}} - \frac{d}{T} \cdot \frac{1}{U_{mr}}. \quad (D3)$$

Collecting terms gives

$$\frac{n_*^{1/2} - 1}{n_*^{3/4} - 1} = \frac{d}{T} \cdot \frac{1}{U_{mr}}. \quad (D4)$$

The r.h.s of the above equation, in terms n_{opt} is

$$\frac{3}{2} n_{opt}^{1/4} = \frac{T}{d} U_{mr}. \quad (D5)$$

Thus equation D4 can be written as

$$\frac{n_*^{3/4} - 1}{n_*^{1/2} - 1} = \frac{3}{2} n_{opt}^{1/4}. \quad (D6)$$

Solving for n_{opt} gives

$$n_{opt} = \frac{16}{81} \left[\frac{n_*^{3/4} - 1}{n_*^{1/2} - 1} \right]^4. \quad (D7)$$

While it is not possible to solve for n_* in the above equation, an upper bound for this variable can be calculated since the denominator, $n_*^{1/2} - 1$, is less than $n_*^{1/2}$

$$n_{opt} > \frac{16}{81} \left[\frac{n_*^{3/4} - 1}{n_*^{1/2}} \right]^4. \quad (D8)$$

Furthermore, $n_*^{1/4} - \frac{1}{\sqrt{n_*}} < n_*^{1/4}$ it follows that

$$n_{opt} > \frac{16}{81} \left[n_*^{1/4} - \frac{1}{n_*^{1/2}} \right]^4 < \frac{16}{18} \left[n_*^{1/4} \right]^4. \quad (D9)$$

Finally, the upper bound for n_* can be written as

$$\frac{81}{16} \cdot n_{opt} > n_*. \quad (D10)$$